



## Supplementary Materials for

### Partitioning of cancer therapeutics in nuclear condensates

Isaac A. Klein\*, Ann Boija\*, Lena K. Afeyan, Susana Wilson Hawken, Mengyang Fan, Alessandra Dall'Agnese, Ozgur Oksuz, Jonathan E. Henninger, Krishna Shrinivas, Benjamin R. Sabari, Ido Sagi, Victoria E. Clark, Jesse M. Platt, Mrityunjay Kar, Patrick M. McCall, Alicia V. Zamudio, John C. Manteiga, Eliot L. Coffey, Charles H. Li, Nancy M. Hannett, Yang Eric Guo, Tim-Michael Decker, Tong Ihn Lee, Tinghu Zhang, Jing-Ke Weng, Dylan J. Taatjes, Arup Chakraborty, Phillip A. Sharp, Young Tae Chang, Anthony A. Hyman, Nathanael S. Gray, Richard A. Young†

\*These authors contributed equally to this work.

†Corresponding author. Email: [young@wi.mit.edu](mailto:young@wi.mit.edu)

Published 19 June 2020, *Science* **368**, 1386 (2020)

DOI: 10.1126/science.aaz4427

#### **This PDF file includes:**

Materials and Methods

Figs. S1 to S30

References

#### **Other Supplementary Material for this manuscript includes the following:**

(available at [science.sciencemag.org/content/368/6497/1386/suppl/DC1](http://science.sciencemag.org/content/368/6497/1386/suppl/DC1))

MDAR Reproducibility Checklist (PDF)

## Materials and Methods

### Cell lines

Cell lines were obtained as indicated, TamR7 (ECACC 16022509). V6.5 murine embryonic stem cells were a gift from R. Jaenisch of the Whitehead Institute. V6.5 are male cells derived from a C57BL/6(F) x 129/sv(M) cross. MCF7 cells were a gift from the R. Weinberg of the Whitehead Institute and HCT116 cells were from ATCC (CCL-247) were used. V6.5 murine embryonic stem endogenously tagged with MED1-mEGFP (*10*), BRD4-mEGFP (*10*), SRSF2-mEGFP (*11*), or HP1 $\alpha$ -mEGFP were used. Cells were tested negative for mycoplasma. The CRISPR/Cas9 system was used to generate genetically modified endogenously tagged ESCs and HCT116 cells. Target-specific sequences were cloned into a plasmid containing sgRNA backbone, a codon-optimized version of Cas9, and BFP or mCherry. A homology directed repair template was cloned into pUC19 using NEBuilder HiFi DNA Master Mix (NEB E2621S). The homology repair template consisted of mCherry or mEGFP cDNA sequence flanked on either side by 800 bp homology arms amplified from genomic DNA using PCR. To generate genetically modified cell lines, 750,000 cells were transfected with 833 ng Cas9 plasmid and 1,666 ng non-linearized homology repair template using Lipofectamine 3000 (Invitrogen L3000). Cells were sorted 48 hours after transfection for the presence of BFP or mCherry fluorescence proteins encoded on the Cas9 plasmid to enrich for transfected cells. This population was allowed to expand for 1 week before sorting a second time for the presence of mCherry or mEGFP. For mES cells, 40,000 mCherry positive cells were plated in serial dilution in a 6-well plate and allowed to expand for a week before individual colonies were manually picked into a 96-well plate. 24 colonies were screened for successful targeting using PCR genotyping to confirm insertion. For HCT116, single cells were

plated in a 96 well plate and allowed to grow until confluence, then screened for successful targeting using PCR genotyping to confirm insertion.

PCR genotyping was performed using Phusion polymerase (Thermo Scientific F531S). Products were amplified according to kit recommendations and visualized on a 1% agarose gel. The following primers were used for PCR genotyping:

HP1 $\alpha$ -mCherry\_fwd (mES): AACGTGAAGTGTCCACAGATTG

HP1 $\alpha$ -mCherry\_rev (mES): TTATGGATGCGTTTAGGATGG

HP1 $\alpha$ -GFP\_fwd (HCT116): CCAAGGTGAGGAGGAAATCA

HP1 $\alpha$ -GFP\_rev (HCT116): CACAGGGAAGCAGAAGGAAG

MED1 $\alpha$ -GFP\_fwd (HCT116): GAAGTTGAGAGTCCCCATCG

MED1-GFP\_rev (HCT116): CGAGCACCCCTTCTCTTCTTG

BRD4-GFP\_fwd (HCT116): CTGCCTCTTGGGCTTGTTAG

BRD4-GFP\_rev (HCT116): TTTGGGGAGAGGAGACATTG

SRSF2-GFP\_fwd (HCT116): CAAGTCTCCTGAAGAGGAAGGA

SRSF2-GFP\_rev (HCT116): AAGGGCTGTATCCAAACAAAAC

FIB1-GFP\_fwd (HCT116): CCTTTTAATCAGCAACCCACTC

FIB1-GFP\_rev (HCT116): GTGACCGAGTGAGAATTTACCC

NPM1-GFP\_fwd (HCT116): TCAAATTCCTGAGCTGAAGTGA

NPM1-GFP\_rev (HCT116): AACACGGTAGGGAAAGTTCTCA

### Cell culture

V6.5 murine embryonic stem (mES) cells were grown in 2i + LIF conditions. mES cells were grown on 0.2% gelatinized (Sigma, G1890) tissue culture plates. The media used for 2i + LIF media conditions is as follows: 967.5 mL DMEM/F12 (GIBCO 11320), 5 mL N2 supplement (GIBCO 17502048), 10 mL B27 supplement (GIBCO 17504044), 0.5mM L-glutamine (GIBCO 25030), 0.5X non-essential amino acids (GIBCO 11140), 100 U/mL Penicillin-Streptomycin (GIBCO 15140), 0.1 mM β-mercaptoethanol (Sigma), 1 uM PD0325901 (Stemgent 04- 0006), 3 uM CHIR99021 (Stemgent 04-0004), and 1000 U/mL recombinant LIF (ESGRO ESG1107). TrypLE Express Enzyme (Life Technologies, 12604021) was used to detach cells from plates. TrypLE was quenched with FBS/LIF-media ((DMEM K/O (GIBCO, 10829-018), 1X nonessential amino acids, 1% Penicillin Streptomycin, 2mM L-Glutamine, 0.1mM β-mercaptoethanol and 15% Fetal Bovine Serum, FBS, (Sigma Aldrich, F4135)). Cells were spun at 1000rpm for 3 minutes at RT, resuspended in 2i media and  $5 \times 10^6$  cells were plated in a 15 cm dish.

MCF7 cells and HCT116 cells were grown in complete DMEM media (DMEM (Life Technologies 11995073), 10% Fetal Bovine Serum, FBS, (Sigma Aldrich, F4135), 1% L-glutamine (GIBCO, 25030-081), 1% Penicillin Streptomycin (Life Technologies, 15140163)). For growth in estrogen-free conditions MCF7 cells in regular media were washed 3x with PBS then the media was changed to estrogen free media containing phenol red-free DMEM (Life Technologies 21063029), 10% charcoal stripped FBS (Life Technologies A3382101), 1% L-glutamine (GIBCO, 25030-081) and 1% Penicillin Streptomycin (Life Technologies, 15140163) for 48 hours prior to use. TamR7 cells were grown in TAMR7 media (Phenol red-free DMEM/F12 (Life Technologies 21041025), 1% L-glutamine (GIBCO, 25030-081) 1% Penicillin Streptomycin (Life Technologies, 15140163), 1% Fetal Bovine Serum, FBS, (Sigma Aldrich, F4135), 6ng/mL insulin (Santa Cruz Biotechnology,

sc-360248)). For passaging, cells were washed in PBS (Life Technologies, AM9625). TrypLE Express Enzyme (Life Technologies, 12604021) was used to detach cells from plates. TrypLE was quenched with indicated media.

### Live cell imaging

Cells were grown on glass dishes (Mattek P35G-1.5-20-C). Before imaging the cells, culture medium was replaced with phenol red-free media, and imaged using the Andor Revolution Spinning Disk Confocal microscope. Raw Andor images were processed using FIJI. For imaging mESC, coated glass dishes were used (5 µg/ml of poly-L-ornithine (Sigma-Aldrich, P4957) for 30 minutes at 37 °C, and with 5 µg/ml of laminin (Corning, 354232) for 2–16 hours at 37 °C). For imaging FIB1 and NPM1 in mES cells, vectors encoding GFP-tagged NPM1 or FIB1 were transfected as described above with Lipofectamine 3000 per package instructions.

### Immunofluorescence of tissue samples

Fresh frozen breast and colon tissues were purchased from BioIVT. Frozen breast tissue was fixed in 2% PFA in PBS for 30minutes-1hour. Fixed tissue was incubated in 30% sucrose in PBS at 4°C for 4 days. Tissue was embedded in OCT and frozen. Fresh frozen colon tissue was embedded in OCT and frozen. Tissue was sectioned into 10µm sections using the cryostat with temperature set at -25°C or -30°C. Sections were stored at -20°C. For IF, sections were brought to room temperature, they were fixed in 4% PFA in PBS for 10 minutes. Following three washes in PBS, tissues were permeabilized using 0.5%TX100 in PBS, washed three times in PBS and blocked with 4% BSA in PBS for 30 minutes. Primary antibodies were diluted into 4% BSA in PBS and added to the tissue sample for O/N incubation at RT. Following three washes in PBS, samples

were incubated with secondary antibodies diluted 1:500 in 4% BSA in PBS. Samples were washed in PBS, DNA was stained using 20 $\mu$ m/mL Hoechst 33258 (Life Technologies, H3569) for 5 minutes and mounted using Vectashield (VWR, 101098-042). Images were acquired using the Elyra Super-Resolution Microscope at Harvard Center for Biological Imaging. Images were post-processed using Fiji Is Just ImageJ (<https://fiji.sc/>).

### Nuclear volume quantification of condensates

For image acquisition: 10 z-slices were imaged. The outline of the nuclei were defined manually in Fiji Is Just ImageJ (<https://fiji.sc/>) and the volume of each nucleus was calculated as nuclear area ( $\mu$ m<sup>2</sup>) \* number of z-slices imaged (10) \* voxel depth (0.1 $\mu$ m). The volume of condensates in the nucleus was measured using a custom Python script and the scikit-image package. Condensates were segmented from 3D images of the protein channel on two criteria: (1) an intensity threshold that was three s.d. above the mean of the image; (2) size thresholds (10 pixel minimum condensate size). The estimated volume of the segmented objects was then calculated by multiplying the width ( $\mu$ m) \* height ( $\mu$ m) \* voxel depth (0.1 $\mu$ m). For each protein factor, the average and s.d. volume of condensates in the healthy and malignant tissue was reported. The number of condensates per nucleus was defined as the number of segmented objects contained within the perimeter of the defined nucleus. For each protein factor, the average and s.d. number of condensates per nucleus in the healthy and malignant tissue was reported. Percentage of nuclear volume occupied by the condensates was calculated as follows: ( $\Sigma$  volume of all detected condensates in the nucleus)/(estimated nuclear volume).

### Antibodies

The following antibodies were used for Immunofluorescence: NPM1 (Abcam ab10530), BRD4 (ab128874), MED1 (ab64965), HP1 $\alpha$  (ab109028), FIB1 (ab5821), SRSF2 (ab11826), ER (ab32063), CDK7 (Santa Cruz sc-7344), Cisplatin modified DNA (ab103261), 568 goat anti rat (Life Technologies A11077), Goat anti-Rabbit IgG Alexa Fluor 488 (Life Technologies A11008).

### Protein purification

Human cDNA was cloned into a modified version of a T7 pET expression vector. The base vector was engineered to include a 5' 6xHIS followed by either BFP, mEGFP or mCherry and a 14 amino acid linker sequence "GAPGSAGSAAGGSG." NEBuilder® HiFi DNA Assembly Master Mix (NEB E2621S) was used to insert these sequences (generated by PCR) in-frame with the linker amino acids. All expression constructs were sequenced to ensure sequence identity.

For protein expression plasmids were transformed into LOBSTR cells (gift of Chessman Lab) and grown as follows. A fresh bacterial colony containing the tagged MED1 constructs were inoculated into LB media containing kanamycin and chloramphenicol and grown overnight at 37°C. Cells were diluted 1:30 in 500ml room temperature LB with freshly added kanamycin and chloramphenicol and grown 1.5 hours at 16°C. IPTG was added to 1mM and growth continued for 20 hours. Cells were collected and stored frozen. Cells containing all other expression plasmids were treated in a similar manner except they were grown for 5 hours at 37°C after IPTG induction.

Cell pellets of SRSF2 were resuspended in 15ml of denaturing buffer (50mM Tris 7.5, 300mM NaCl, 10mM imidazole, 8M Urea) with cOmplete protease inhibitors (Roche,11873580001) and sonicated (ten cycles of 15 seconds on, 60 sec off). The lysates were cleared by centrifugation at

12,000g for 30 minutes and added to 1ml of Ni-NTA agarose (Invitrogen, R901-15) that had been pre-equilibrated with 10 volumes of the same buffer. Tubes containing this agarose lysate slurry were rotated for 1.5 hours at room temperature, then centrifuged for 10 minutes at 3,000 rpm, washed with 2 X 5ml of lysis buffer and eluted with 3 X 2ml lysis buffer with 250mM imidazole. Elutions were incubated for at least 10 minutes rotating at room temperature and centrifuged for 10 minutes at 3,000 rpm to collect protein. Fractions were run on a 12% acrylamide gel and proteins of the correct size were dialyzed first against buffer containing 50mM Tris pH 7.5, 500mM NaCl, 1Mm DTT and 4M Urea, followed by the same buffer containing 2M Urea and lastly 2 changes of buffer with 10% Glycerol, no Urea. Any precipitate after dialysis was removed by centrifugation at 3,000rpm for 10 minutes. All other proteins were purified in a similar manner by resuspending cell pellets in 15ml of buffer containing 50mM Tris pH7.5, 500 mM NaCl, cOmplete protease inhibitors, sonicating, and centrifuging at 12,000xg for 30 minutes at 4°C. The lysate was added to 1ml of pre-equilibrated Ni-NTA agarose, and rotated at 4°C for 1.5 hours. The resin slurry was centrifuged at 3,000 rpm for 10 minutes, washed with 2 X 5ml lysis buffer with 50mM imidazole and eluted by incubation for 10 or more minutes rotating 3 X with 2ml lysis buffer containing 250mM imidazole followed by centrifugation and gel analysis. Fractions containing protein of the correct size were dialyzed against two changes of buffer containing 50mM Tris 7.5, 125mM NaCl, 10% glycerol and 1mM DTT at 4°C or the same buffer with 500mM NaCl for the HP1 $\alpha$  construct.

The following human proteins or protein fragments were used for production:

NPM1 - full length, amino acids 1-294.

SRSF2 - full length, amino acids 1-221.

HP1 $\alpha$  - full length, amino acids 1-191.

MED1 - amino acids 600-1581.

MED1 - aromatic mutant amino acids 600-1581, all aromatic residues changed to alanine.

MED1 - basic mutant amino acids 600-1581, all basic residues changed to alanine.

BRD4 - amino acids 674-1351.

FIB1- full length, amino acids 1-321.

ER and ER mutants - full length, amino acids 1-595 (WT).

### Cbioportal data acquisition

For frequency of patient mutations, cbioportal (<http://www.cbioportal.org/>) was queried for mutations in ESR1 that are present in any breast cancer sequencing data set.

### Drugs and small molecules

Drugs and small molecules were obtained and processed as follows. Hoescht 33258 (Life Technologies H3569) was obtained and utilized in liquid form, Fluorescein (Sigma F2456) was dissolved in DMSO at 10mM then diluted further in droplet formation buffer for use. Dextrans measuring 4.4kDa (Sigma T1037), 10kDa (Invitrogen D1816), 40kDa (Invitrogen D1842), or 70kDa (Invitrogen D1864) conjugated to either TRITC or FITC, ROX (Life technologies 12223012), and Texas Red (Sigma Aldrich 60311-02-6), were diluted in droplet formation buffer. FLTX1 (AOBIO 4054) was dissolved in DMSO then diluted further in droplet formation buffer. THZ1-TMR and JQ1-ROX was synthesized as below to achieve the molecular structure displayed in Figure 2D-E. Cisplatin conjugated to texas red (Ursa Bioscience) was dissolved in DMF to 2mM and diluted for further use in droplet formation buffer. Mitoxantrone (Sigma F6545) was dissolved

in DMSO and diluted for further use in droplet formation buffer. Chemical structures were made using ChemDraw software.

Unlabeled molecules were used for live cell and chase out experiments as below: JQ1 (Cayman Chemical 11187), cisplatin (Selleck S1166), transplatin (Toku-E T108), tamoxifen (Sigma Aldrich T5648), 4-hydroxytamoxifen (Sigma H7904).

### In vitro droplet assay

Recombinant BFP, GFP, or mCherry fusion proteins were concentrated and desalted to an appropriate protein concentration and 125mM NaCl using Amicon Ultra centrifugal filters (30K MWCO, Millipore). Recombinant protein was added to droplet formation buffer (50mM Tris-HCl pH 7.5, 10% glycerol, 1mM DTT) with the indicated amount of salt and the indicated crowding agent (Ficoll or PEG). The protein solution was immediately loaded onto glass bottom 384 well plate (Cellvis P384-1.5H-N) and imaged with an Andor confocal microscope with a 150x objective. Unless indicated, images presented are of droplets settled on the glass coverslip. For each experiment at least 10 images were taken. Images were post-processed using Fiji Is Just ImageJ (<https://fiji.sc/>).

Drug and small molecule concentrations used in the droplet experiments are as follows:

Texas red-cisplatin - 5 $\mu$ M

FLTX1 - 100 $\mu$ M

Mitoxantrone - 50 $\mu$ M

Fluorescein - 1 $\mu$ M

Hoechst - 1mg/mL

Labeled dextrans - 0.05mg/mL

THZ1-TMR - 5 $\mu$ M

JQ1-ROX - 1 $\mu$ M

ROX - 1 $\mu$ M

TR - 5 $\mu$ M

For chase-out experiments 5 $\mu$ M labeled cisplatin-TR was added to a MED1 droplet reaction (10  $\mu$ M MED1, 50mM Tris-HCl pH 7.5, 10% glycerol, 1mM DTT, 10% PEG) in order to form MED1 droplets concentrated with Cisplatin-TR. Unlabeled transplatin or unlabeled cisplatin (vehicle, 10 $\mu$ M, 100 $\mu$ M, or 500 $\mu$ M) were added to the droplet mixture and the amount of labeled cisplatin-TR remaining in the droplet is measured after chase out. 100 $\mu$ M fluorescent FLTX1 was added to a MED1 droplet reaction (10  $\mu$ M MED1, 50mM Tris-HCl pH 7.5, 10% glycerol, 1mM DTT, 10% PEG) in order to form MED1 droplets concentrated with FLTX1. 1mM of the non-fluorescent version of the drug, tamoxifen, was added to the droplet mixture and the amount of fluorescent FLTX1 remaining in the droplet is measured after chase out. For assaying eviction of ER from MED1 condensates, fluorescently labeled ER and MED1 were mixed in droplet formation buffer at the indicated concentrations with the indicated components in the presence of 100 $\mu$ M estrogen (Sigma E8875). For conditions with tamoxifen treatment, 4-hydroxytamoxifen (Sigma H7904) was then added to a final concentration of 100 $\mu$ M and imaged as above on a confocal fluorescent microscope. Images were post-processed using Fiji Is Just ImageJ (FIJI).

For droplet assay with fluorescent DNA a 451 basepair DNA fragment was commercially synthesized in a vector with flanking M13F and M13R primer binding sites. Primers M13F and M13R were commercially synthesized covalently bound to a Cy5 fluorophore and this fragment was amplified using these primers. The DNA fragment was then purified from PCR reactions and diluted in droplet formation buffer for use in the droplet assay as described. For testing the ability of recombinant CDK7 to partition in MED1 or HP1 $\alpha$  droplets, recombinant CDK activating complex (Millipore 14-476) was supplied at 0.4mg/mL in 150mM NaCl at pH 7.5. One vial of Cy5 monoreactive dye (Amersham PA23001) was resuspended in 30uL of 0.2M Sodium Bicarbonate at pH 9.3 in 150mM NaCl. 5uL of this reaction was added to 5uL of protein and incubated at RT for 1 hour. Free dye was removed by passing through a Zeba Spin Desalting Columns, 40MWCO (87764, Thermo Scientific) as described in the package insert into droplet formation buffer with 1mM DTT in 125mM NaCl at a final concentration of 1uM. This protein was used in the droplet assay as needed.

For screening of a modified BODIPY library, 81 modified BODIPY molecules were selected from a larger library collection as previous described (56). These molecules were diluted to 1mM in DMSO then to 10 $\mu$ M in droplet formation buffer. Droplets of MED1-IDR-BFP were formed in Droplet formation buffer with 125mM NaCl and 10% PEG with 5 $\mu$ M protein, probe was added to this reaction to a final concentration of 1 $\mu$ M, the mixture was added to one well of a 384-well plate and imaged on an Andor confocal fluorescent microscope at 150x in the 488 (BODIPY) and 405 (protein) channels. Images were post-processed using Fiji Is Just ImageJ (FIJI). Images were quantified by the aforementioned pipelines to quantify the maximum 488 signal intensity in

droplets defined by the 405 channel. These values were then ranked to quantify the top and bottom “hits”. To ensure that the fluorescent intensity of the probes were equivalent, 1  $\mu$ M of 18 random probes in droplet formation buffer was imaged as above and the average fluorescent intensity in the field determined. The same approach was taken to measure the fluorescent intensity of BODIPY alone (Sigma 795526), both in MED1 droplet and in the diffuse state.

#### FRAP of in vitro droplets with drug

For FRAP of in vitro droplets, 5 pulses of laser at a 50  $\mu$ s dwell time was applied to the MED1 channel and 20 pulses of laser at a 100  $\mu$ s dwell time was applied to the Cisplatin channel. Recovery was imaged on an Andor microscope every 1s for the indicated time periods. Fluorescence intensity was measured using FIJI. Post bleach FRAP recovery data was averaged over 6 replicates for each channel.

#### Calculating drug enrichment ratios

To analyze in vitro droplet experiments, custom Python scripts using the scikit-image package were written to identify droplets and characterize their size, shape and intensity. Droplets were segmented from average images of captured channels on various criteria: (1) an intensity threshold that was three s.d. above the mean of the image; (2) size thresholds (20 pixel minimum droplet size); and (3) a minimum circularity ( $\text{circularity} = \frac{4\pi \cdot \text{area}}{\text{perimeter}^2}$ ) of 0.8 (1 being a perfect circle). After segmentation, mean intensity for each droplet was calculated while excluding pixels near the phase interface, and background-corrected by subtracting intensity of dark images of droplet formation buffer only. Droplets identified in the channel of the fluorescent protein from

ten independent fields of view were quantified for each experiment. The maximum intensity of signal within the droplets was calculated for each channel, the maximum intensity in the drug channel was termed “maximum drug intensity”. To obtain the intensity of drug or dye alone in the diffuse state (termed “diffuse drug intensity”), the compound was added to droplet formation buffer at same concentration used in the droplet assay. This was then imaged on a confocal fluorescent microscope, the resulting image was processed in FIJI to obtain the fluorescent intensity of the field. To obtain the fluorescent intensity of protein droplets that bleed through in the drug channel (termed “background intensity”) protein droplets were imaged in the fluorescent channel in which the drug fluoresces and processed as above to obtain the average maximum intensity within the droplet across 10 images. The enrichment ratio was obtained by the following formula  $[(\text{maximum drug intensity}) - (\text{background intensity})] / (\text{diffuse drug intensity})$ . The box plots show the distributions of all droplets. Each dot represents an individual droplet.

#### Chromatin immunoprecipitation (ChIP) and sequencing

MCF7 cells were grown in complete DMEM media to 80% confluence. 1% formaldehyde in PBS was used for crosslinking of cells for 15 minutes, followed by quenching with Glycine at a final concentration of 125mM on ice. Cells were washed with cold PBS and harvested by scraping cells in cold PBS. Collected cells were pelleted at 1000 g for 3 minutes at 4°C, flash frozen in liquid nitrogen and stored at 80°C. All buffers contained freshly prepared cOmplete protease inhibitors (Roche, 11873580001). Frozen crosslinked cells were thawed on ice and then resuspended in lysis buffer I (50 mM HEPES-KOH, pH 7.5, 140 mM NaCl, 1 mM EDTA, 10% glycerol, 0.5% NP-40, 0.25% Triton X-100, protease inhibitors) and rotated for 10 minutes at 4°C, then spun at 1350 rcf., for 5 minutes at 4°C. The pellet was resuspended in lysis buffer II (10 mM Tris-HCl, pH 8.0, 200

mM NaCl, 1 mM EDTA, 0.5 mM EGTA, protease inhibitors) and rotated for 10 minutes at 4°C and spun at 1350 rcf. for 5 minutes at 4°C. The pellet was resuspended in sonication buffer (20 mM Tris-HCl pH 8.0, 150 mM NaCl, 2 mM EDTA pH 8.0, 0.1% SDS, and 1% Triton X-100, protease inhibitors) and then sonicated on a Misonix 3000 sonicator for 10 cycles at 30 s each on ice (18-21 W) with 60 s on ice between cycles. Sonicated lysates were cleared once by centrifugation at 16,000 rcf. for 10 minutes at 4°C. Input material was reserved and the remainder was incubated overnight at 4°C with magnetic beads bound with CDK7 Bethyl A300-405A antibody to enrich for DNA fragments bound by CDK7. Beads were washed twice with each of the following buffers: wash buffer A (50 mM HEPES-KOH pH 7.5, 140 mM NaCl, 1 mM EDTA pH 8.0, 0.1% Na-Deoxycholate, 1% Triton X-100, 0.1% SDS), wash buffer B (50 mM HEPES-KOH pH 7.9, 500 mM NaCl, 1 mM EDTA pH 8.0, 0.1% Na-Deoxycholate, 1% Triton X-100, 0.1% SDS), wash buffer C (20 mM Tris-HCl pH 8.0, 250 mM LiCl, 1 mM EDTA pH 8.0, 0.5% Na-Deoxycholate, 0.5% IGEPAL C-630, 0.1% SDS), wash buffer D (TE with 0.2% Triton X-100), and TE buffer. DNA was eluted off the beads by incubation at 65°C for 1 hour with intermittent vortexing in elution buffer (50 mM Tris-HCl pH 8.0, 10 mM EDTA, 1% SDS). Cross-links were reversed overnight at 65°C. To purify eluted DNA, 200 µL TE was added and then RNA was degraded by the addition of 2.5 µL of 33 mg/mL RNase A (Sigma, R4642) and incubation at 37°C for 2 hours. Protein was degraded by the addition of 10 µL of 20 mg/mL proteinase K (Invitrogen, 25530049) and incubation at 55°C for 2 hours. A phenol:chloroform:isoamyl alcohol extraction was performed followed by an ethanol precipitation. The DNA was then resuspended in 50 µL TE and used for sequencing. ChIP libraries were prepared with the Swift Biosciences Accel-NGS 2S Plus DNA Library Kit, according to the kit instructions. Following library preparation, ChIP libraries were run on a 2% gel on the PippinHT with a size-collection window of 200–600 bases. Final

libraries were quantified by qPCR with the KAPA Library Quantification kit from Roche, and sequenced in single-read mode for 40 bases on an Illumina HiSeq 2500.

HCT116 cells were grown in complete DMEM media to 80% confluence followed by treatment with JQ1 or DMSO for 24 hours, followed by cell permeabilization (10min at 37°C with the solution of tx100 in PBS at 1:1000 in media) and subsequently treated with DMF or Cisplatin for 6 hours. 1% formaldehyde in PBS was used for crosslinking of cells for 15 minutes, followed by quenching with Glycine at a final concentration of 125mM on ice. Cells were washed with cold PBS and harvested by scraping cells in cold PBS. Collected cells were pelleted at 1000 g for 3 minutes at 4°C, flash frozen in liquid nitrogen and stored at -80°C. All buffers contained freshly prepared cOmplete protease inhibitors (Roche, 11873580001). Frozen crosslinked cells were thawed on ice and then resuspended in lysis buffer I (50 mM HEPES-KOH, pH 7.5, 140 mM NaCl, 1 mM EDTA, 10% glycerol, 0.5% NP-40, 0.25% Triton X-100, protease inhibitors) and rotated for 10 minutes at 4°C, then spun at 1350 rcf., for 5 minutes at 4°C. The pellet was resuspended in lysis buffer II (10 mM Tris-HCl, pH 8.0, 200 mM NaCl, 1 mM EDTA, 0.5 mM EGTA, protease inhibitors) and rotated for 10 minutes at 4°C and spun at 1350 rcf. for 5 minutes at 4°C. The pellet was resuspended in sonication buffer (20 mM Hepes pH 7.5, 140 mM NaCl, 1 mM EDTA 1 mM EGTA, 1% Triton X-100, 0.1% Na-deoxycholate, 0.1% SDS, protease inhibitors) and then sonicated on a Misonix 3000 sonicator for 10 cycles at 30 s each on ice (18-21 W) with 60 s on ice between cycles. Sonicated lysates were cleared once by centrifugation at 16,000 rcf. for 10 minutes at 4°C. Input material was reserved and the remainder was incubated overnight at 4°C with magnetic beads bound with MED1 antibody (Bethyl A300-793A) to enrich for DNA fragments bound by MED1. Beads were washed with each of the following buffers: washed twice

with sonication buffer (20 mM Hepes pH 7.5, 140 mM NaCl, 1 mM EDTA 1 mM EGTA, 1% Triton X-100, 0.1% Na-deoxycholate, 0.1% SDS), once with sonication buffer with high salt (20 mM Hepes pH 7.5, 500 mM NaCl, 1 mM EDTA 1 mM EGTA, 1% Triton X-100, 0.1% Na-deoxycholate, 0.1% SDS), once with LiCl wash buffer (20 mM Tris pH 8.0, 1 mM EDTA, 250 mM LiCl, 0.5% NP-40, 0.5% Na-deoxycholate), and once with TE buffer. DNA was eluted off the beads by incubation with agitation at 65°C for 15 minutes in elution buffer (50 mM Tris-HCl pH 8.0, 10 mM EDTA, 1% SDS). Cross-links were reversed for 12 hours at 65°C. To purify eluted DNA, 200 mL TE was added and then RNA was degraded by the addition of 2.5 mL of 33 mg/mL RNase A (Sigma, R4642) and incubation at 37°C for 2 hours. Protein was degraded by the addition of 4 ul of 20 mg/mL proteinase K (Invitrogen, 25530049) and incubated at 55°C for 30 minutes. DNA was purified using Qiagen PCR purification kit, eluted in 30 µl Buffer EB, and used for sequencing. ChIP libraries were prepared with the Swift Biosciences Accel-NGS 2S Plus DNA Library Kit, according to the kit instructions. Following library preparation, ChIP libraries were run on a 2% gel on the PippinHT with a size-collection window of 200–400 bases. Final libraries were quantified by qPCR with the KAPA Library Quantification kit from Roche, and sequenced in single-read mode for 50 bases on an Illumina HiSeq 2500.

ChIP-Seq data were aligned to the mm9 version of the mouse reference genome using bowtie with parameters `-k 1 -m 1 -best` and `-l` set to read length. Wiggle files for display of read coverage in bins were created using MACS with parameters `-w -S -space = 50 -nomodel -shiftsize = 200`, and read counts per bin were normalized to the millions of mapped reads used to make the wiggle file. Reads-per-million-normalized wiggle files were displayed in the UCSC genome browser. For

ER, MED1, BRD4, and H3K9me3 ChIP-Seq in MCF7 cells, published datasets were used (GEO GSE60270, GSM1348516, and GSM945857, respectively).

#### Purification of CDK8-Mediator

The CDK8-Mediator samples were purified as described (57) with modifications. Prior to affinity purification, the P0.5M/QFT fraction was concentrated, to 12 mg/mL, by ammonium sulfate precipitation (35%). The pellet was resuspended in pH 7.9 buffer containing 20mM KCl, 20mM HEPES, 0.1mM EDTA, 2mM MgCl<sub>2</sub>, 20% glycerol and then dialyzed against pH 7.9 buffer containing 0.15M KCl, 20mM HEPES, 0.1mM EDTA, 20% glycerol and 0.02% NP-40 prior to the affinity purification step. Affinity purification was carried out as described, eluted material was loaded onto a 2.2mL centrifuge tube containing 2mL 0.15M KCl HEMG (20mM HEPES, 0.1mM EDTA, 2mM MgCl<sub>2</sub>, 10% glycerol) and centrifuged at 50K RPM for 4h at 4°C. This served to remove excess free GST-SREBP and to concentrate the CDK8-Mediator in the final fraction. Prior to droplet assays, purified CDK8-Mediator was concentrated using Microcon-30kDa Centrifugal Filter Unit with Ultracel-30 membrane (Millipore MRCF0R030) to reach 300nM of Mediator complex. Concentrated CDK8-Mediator was added to the droplet assay to a final concentration of 200nM. Droplet reactions contained 10% PEG-8000 and 125mM salt.

#### Immunofluorescence with RNA FISH

Cells were plated on coverslips and grown for 24 hours followed by fixation using 4% paraformaldehyde, PFA, (VWR, BT140770) in PBS for 10 minutes. After washing cells three times in PBS, the coverslips were put into a humidifying chamber or stored at 4°C in PBS. Permeabilization of cells were performed using 0.5% Triton X-100 (Sigma Aldrich, X100) in PBS

for 10 minutes followed by three PBS washes. Cells were blocked with 4% IgG-free Bovine Serum Albumin, BSA, (VWR, 102643-516) for 30 minutes and the indicated primary antibody (see table S2) was added at a concentration of 1:500 in PBS for 4-16 hours. Cells were washed with PBS three times followed by incubation with secondary antibody at a concentration of 1:5000 in PBS for 1 hour. After washing twice with PBS, cells were fixed using 4% paraformaldehyde, PFA, (VWR, BT140770) in PBS for 10 minutes. After two washes of PBS, Wash buffer A (20% Stellaris RNA FISH Wash Buffer A (Biosearch Technologies, Inc., SMF-WA1-60), 10% Deionized Formamide (EMD Millipore, S4117) in RNase-free water (Life Technologies, AM9932) was added to cells and incubated for 5 minutes. 12.5 mM RNA probe (Stellaris) in Hybridization buffer (90% Stellaris RNA FISH Hybridization Buffer (Biosearch Technologies, SMF-HB1-10) and 10% Deionized Formamide) was added to cells and incubated overnight at 37°C. After washing with Wash buffer A for 30 minutes at 37°C, the nuclei were stained with 20 mg/mL Hoechst 33258 (Life Technologies, H3569) for 5 minutes, followed by a 5 minute wash in Wash buffer B (Biosearch Technologies, SMF-WB1-20). Cells were washed once in water followed by mounting the coverslip onto glass slides with Vectashield (VWR, 101098-042) and finally sealing the coverslip with nail polish (Electron Microscopy Science Nm, 72180). Images were acquired at an RPI Spinning Disk confocal microscope with a 100x objective using MetaMorph acquisition software and a Hamamatsu ORCA-ER CCD camera (W.M. Keck Microscopy Facility, MIT). Images were post-processed using Fiji Is Just ImageJ (FIJI).

### RNA FISH image analysis

For analysis of RNA FISH with immunofluorescence, custom Python scripts were written to process and analyze 3D image data gathered in FISH and immunofluorescence channels. FISH

foci were automatically called using the scipy ndimage package. The ndimage find\_objects function was then used to call contiguous FISH foci in 3D. These FISH foci were then filtered by various criteria, including size, circularity of a maximum z-projection ( $\text{circularity} = \frac{4\pi \cdot \text{area}}{\text{perimeter}^2}$ ; 0.7), and being present in a nucleus (determined by nuclear mask). The FISH foci were then centered in a 3D box (length size ( $l$ ) = 3.0  $\mu\text{m}$ ). The immunofluorescence signals centered at FISH foci for each FISH and immunofluorescence pair were then combined, and an average intensity projection was calculated, providing averaged data for immunofluorescence signal intensity within a  $l \times l$  square centered at FISH foci. As a control, this same process was carried out for immunofluorescence signals centered at an equal number of randomly selected nuclear positions. These average-intensity projections were then used to generate 2D contour maps of the signal intensity. Contour plots were generated using the matplotlib Python package. For the contour plots, the intensity-color ranges presented were customized across a linear range of colors ( $n = 15$ ). For the FISH channel, black to magenta was used. For the immunofluorescence channel, we used chroma.js (an online color generator) to generate colors across 15 bins, with the key transition colors chosen as black, blue-violet, medium blue and lime. This was done to ensure that the reader's eye could more-readily detect the contrast in signal. The generated color map was used in 15 evenly spaced intensity bins for all immunofluorescence plots. The averaged immunofluorescence, centered at FISH or at randomly selected nuclear locations, is plotted using the same color scale, set to include the minimum and maximum signal from each plot.

### Cisplatin treatments followed by immunofluorescence

HCT116 cells were plated in 24-well plate at 50k cells per well to yield 100k cells after 21 hours (doubling time of HCTs). Cells were permeabilized using a solution of Tx100 in media at 0.55 pmol/cell for 12 minutes at 37°C. Cells were then washed with 500 µl media and treated with 500 µl of 50 µM cisplatin in media for 6 hours. After 6 hours, the cells were washed once with room temperature PBS and then fixed with 500 µL 4% formaldehyde in PBS for 12 min at room temperature. The cells were then washed 3 more times with PBS. Coverslips were put into a humidifying chamber or stored at 4°C in PBS. Permeabilization of cells were performed using 0.5% Triton X-100 (Sigma Aldrich, X100) in PBS for 10 minutes followed by three PBS washes. Cells were blocked with 4% IgG-free Bovine Serum Albumin, BSA, (VWR, 102643-516) for 30 minutes and the indicated primary antibody was added at a concentration of 1:500 in PBS for 4-16 hours. Cells were washed with PBS three times followed by incubation with secondary antibody at a concentration of 1:5000 in PBS for 1 hour. Samples was washed in PBS, DNA was stained using 20µm/mL Hoechst 33258 (Life Technologies, H3569) for 5 minutes and mounted using Vectashield (VWR, 101098-042). Images were acquired at an RPI Spinning Disk confocal microscope with a 100x objective using MetaMorph acquisition software and a Hamamatsu ORCA-ER CCD camera (W.M. Keck Microscopy Facility, MIT). Images were post-processed using Fiji Is Just ImageJ (FIJI).

### Cisplatin/condensate co-IF

For the analysis of co-immunofluorescence data, custom python scripts were written to both process and analyze the 3D image data from IF and DAPI channels. Nuclei were detected using the Triangle thresholding method and a nuclear mask was applied the IF channels. Manual minimal thresholds were applied to the 488 channel to determine nuclear puncta for protein of interest

(MED1, HP1a, or FIB1). The triangle thresholding method was applied to the 561 channel to determine nuclear puncta for cisplatin. Percentage of cisplatin overlap was calculated by the number of defined nuclear cisplatin puncta that overlapped with the protein of interest puncta divided by the total number of nuclear cisplatin puncta.

### Cisplatin-seq analysis

Cisplatin-seq fastq files for rep1 24-hour treated cells were downloaded from [https://www.ncbi.nlm.nih.gov/sra/SRX1962532\[accn\]](https://www.ncbi.nlm.nih.gov/sra/SRX1962532[accn]) (sequencing run ID SRR3933212) (40). Reads were aligned to the human genome build hg19 (GRCh37) using Bowtie2 to get aligned .bam files (58). H3K27Ac ChIP-seq reads in HELA cells were used to call super-enhancers using the ROSE algorithm (47, 59). Super-enhancers were separated from typical enhancers using the super-enhancer table output by ROSE algorithm. The typical enhancers were broken down further by their H3K27Ac signal. The last decile of enhancers was extracted based on H3K27Ac signal to get the low H3K27Ac category of enhancers. Each category of enhancer (super-enhancers, typical enhancers, and low H3K27Ac signal enhancers) was broken down into their constituents, and constituents that overlapped with blacklist regions were excluded. Black list regions were downloaded from ENCODE file <https://www.encodeproject.org/files/ENCFF001TDO/>. Each enhancer constituent was then extended by 2kb at either end. The 24-hour treated cisplatin-seq reads were mapped to each of the three categories of 2kb-extended enhancers using the bamToGFF.py script. For each category of enhancer, the constituent region and flanking regions were separately split into 50 equally-sized bins and the reads in each bin were counted. The average read count per bin across all enhancer constituents and flanking regions was used to create the meta-plot.

### Cisplatin Treatments followed by live cell imaging

HCT116 cells with the indicated GFP knock-in were plated at 35k per well of a glass bottom 8-well chamber slide. Following incubation at 37°C overnight, cells were treated with 50µM cisplatin in DMEM or a 1:1000 dilution of DMSO for 12 hours. Prior to imaging, cells were additionally treated with a 1:5000 dilution of Hoechst 33342 to stain DNA and 2µM propidium iodide to stain dead cells. For the quantified dataset of GFP-tagged MED1, HP1 or FIB1 in HCT116 cells, cells were imaged using an Andor confocal microscope at 100X magnification. For representative images of each of the six tagged lines treated with vehicle or 50µM cisplatin, cells were imaged on the Zeiss LSM 880 confocal microscope with Airyscan detector with 63x objective at 37°C. Images were post-processed using Fiji Is Just ImageJ (FIJI).

### Condensate score analysis

Nuclei were segmented from images of treated cells by custom Python scripts using the *scikit-image*, *open-cv*, and *scipy-ndimage* Python packages. Nuclei were segmented by median filter, thresholding, separated by the watershed algorithm, and labeled by the *scikit-image label* function. For each nuclei, the fluorescence signal in the GFP channel (corresponding to either MED1, HP1α or FIB1) was maximally-projected if z-stacks were acquired. A grey-level co-occurrence matrix (GLCM) was then generated from the projected signal, and the ‘correlation’ texture property from the GLCM was calculated per nucleus. One-way ANOVA followed by Sidak’s multiple comparisons test was performed on the correlation values across conditions using GraphPad Prism version 8.2.0 for Mac ([www.graphpad.com](http://www.graphpad.com)). Finally, to derive the condensation score, these values were subtracted from 1.

### FRAP of HCT116 mEGFP tagged cell lines

FRAP was performed on Andor confocal microscope with 488nm laser. Bleaching was performed over a  $r_{bleach} \approx 1 \mu m$  using 100% laser power and images were collected every two seconds. Fluorescence intensity was measured using FIJI. Background intensity was subtracted, and values are reported relative to pre-bleaching time points. Post bleach FRAP recovery data was averaged over 7 replicates for each cell-line and condition.

### Determination of partitioning by spectrophotometry and quantitative phase microscopy

#### *Derivation of expression for drug partition coefficient in condensates*

Here we derive briefly an expression for the partition coefficient of a client molecule into a condensed phase in terms of quantities that are readily measurable experimentally. We consider a sample composed of two coexisting phases, named dilute and condensed, with volume fractions  $\phi_{dilute}$  and  $\phi_{cond}$  such that  $\phi_{dilute} + \phi_{cond} = 1$ . If a client molecule (e.g. a drug) is also present in the sample at an average concentration of  $c_{total}$ , then mass conservation requires that

$$c_{total} = c_{dilute}\phi_{dilute} + c_{cond}\phi_{cond}, \quad (1)$$

where  $c_{dilute}$  and  $c_{cond}$  are the concentrations of the client in the dilute and condensed phases, respectively. Finally, we define the partition coefficient of the client into the condensed phase as  $P = c_{cond}/c_{dilute}$ . With this definition and the requirement that the phase volume fractions sum to 1, Eq 1 can be written as

$$c_{total} = c_{dilute}(1 - \phi_{cond}) + c_{dilute}P\phi_{cond}, \quad (2)$$

which can be simplified and rearranged to yield

$$P = 1 + \left(\frac{c_{total}}{c_{dilute}} - 1\right)(\phi_{cond})^{-1}. \quad (3)$$

We estimate the ratio  $c_{total}/c_{dilute}$  from fluorescence spectroscopy measurements, as described in a subsequent section, while  $\phi_{cond}$  we infer from the lever rule (60) as follows: denoting the concentration of scaffold protein (e.g. MED1) by  $s$ , mass conservation gives  $s_{total} = s_{dilute}\phi_{dilute} + s_{cond}\phi_{cond}$ , in analogy with Eq. 1. Again using the requirement that the volume fractions of coexisting phases sum to 1, this can be rearranged to yield

$$\phi_{cond} = \frac{s_{total} - s_{dilute}}{s_{cond} - s_{dilute}}, \quad (4)$$

where  $s_{total}$  and  $s_{dilute}$  are measured spectrophotometrically from optical absorbance at 280 nm, and  $s_{cond}$  is measured from quantitative phase microscopy, using a coherence-controlled holographic microscope (Q-Phase, Telight (formerly TESCAN), Brno, CZ) equipped with 40x dry objectives (NA = 0.90).

#### *UV-Vis fluorescence spectroscopy measurements and analysis*

Uv-vis spectroscopy (TECAN Spark20M) was used to estimate the absolute concentration of drug in solution using Beer-Lambert law with Eq 5,

$$A = \text{Log}_{10}(I_0/I) = \epsilon cL \quad (5)$$

where A is the measured absorbance (in Absorbance Units (AU)),  $I_0$  is the intensity of the incident light at a given wavelength, I is the transmitted intensity, L the path length through the sample, and c the concentration of the absorbing species. For each species and wavelength,  $\epsilon$  is a constant known as the molar absorptivity or extinction coefficient. This constant is a fundamental molecular property in a given solvent, at a particular temperature and pressure, and has units of  $1/M \cdot \text{cm}$ .

The partitioned drug was measured by using spin down assay. Known concentration of drug was added with the protein and kept for the droplet formation. After 30 minutes, the mixture was centrifuged at 15,000 rpm for 10 minutes. The supernatant was collected and measured the

concentrations of the drug. The partitioned drug was calculated by subtracting from the total known concentration of drug added.

### *Quantitative phase microscopy measurements and analysis*

Quantitative phase measurements were performed using a coherence-controlled holographic microscope (Q-Phase, Telight (formerly TESCAN), Brno, CZ) equipped with 40x dry objectives (NA = 0.90) as follows. Immediately following phase separation, samples were loaded into a custom temperature-controlled flowcell, sealed and allowed to settle under gravity prior to imaging. Flowcells were constructed with a PEGylated coverslip and a sapphire slide as bottom and top surfaces, respectively, using parafilm strips as spacers. Peltier elements affixed to the sapphire slide enabled regulation of flowcell temperature, as previously described (61). Temperature was maintained at  $21.00 \pm 0.02$  °C during measurements.

Q-PHASE software was used to construct compensated phase images from acquired holograms, which were subsequently analyzed in MATLAB using custom code. As details regarding the calculation of protein concentration from quantitative phase images will be discussed extensively elsewhere (McCall et al, forthcoming), only a conceptual overview will be given here. Briefly, each phase image is spatially segmented based on intensity, and a window containing each segmented object is fit to a spatial function of the form

$$\varphi(x, y) = \frac{2\pi}{\lambda} \Delta n H(x, y|R), \quad (6)$$

where  $\varphi(x, y)$  is the phase intensity at pixel location  $(x, y)$ ,  $\lambda$  is the illumination wavelength,  $\Delta n$  is the refractive index difference between MED1 condensates and the surrounding dilute phase, and  $H(x, y|R)$  is the projected height of a sphere of radius  $R$ . The fitting parameters in Eq. 6 are

$\Delta n$  and  $R$ . We assume that no PEG partitions into the condensates and calculate the average scaffold concentration in each filtered condensate as

$$s_{cond} = \frac{\Delta n + (n_{dilute} - n_0)}{dn/ds}. \quad (7)$$

Here  $n_0$  is the refractive index of buffer in the absence of scaffold and PEG,  $n_{dilute}$  is the refractive index of the dilute phase, and both are measured at  $21.00 \pm 0.01$  °C using a J457 digital refractometer (Rudolph Research Analytic, Hackettstown, NJ). The refractive index increment of the scaffold protein,  $dn/ds$ , is estimated from amino acid composition (62).

#### Cisplatin-DNA engagement assay

MED1-IDR-BFP and HP1a-BFP droplets were formed by mixing 10  $\mu$ M protein with the droplet formation buffer containing 50mM Tris-HCl pH 7.5, 100mM NaCl, 10% PEG 8000, 10% glycerol, 1mM DTT and 5ng/ $\mu$ l DNA in a 10  $\mu$ l reaction volume. The droplet reactions were incubated for 30 min at RT. Next, increasing concentrations of activated Cisplatin (0, 0.5, 0.75, 1, 1.5, and 2 mM) were added to the droplet reactions and incubated for another 30 min at RT. The reactions are then treated with 1  $\mu$ l of Proteinase K (Invitrogen, 20 mg/ml) for 4 hr at 55 °C. Platination of DNA was visualized by size-shift on a bioanalyzer. Measurements from two chip runs were compiled into a single electropherogram.

#### Amino acid and basic/acidic patch analysis

Basic and acidic patches were determined by identifying charged interaction elements (CIEs) as previously described by (63). For each protein, the net charge per residue (NCPR) along the protein sequence was calculated using a sliding window of 5 amino acids with a step size of 1 amino acid using the localCIDER software (64). Stretches of 4 or more amino acids with NCPR < -0.35 were

identified as acidic patches (CIE-), while stretches of 4 or more amino acids with NCPR > +0.35 were identified as basic patches (CIE+). The number of acidic and basic patches within the total protein and the IDR specifically was counted. Separately, the number of aromatic residues within the whole protein and the IDR was also counted.

### Cell survival assay

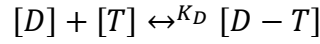
HCT116 cells were plated in 24-well plate at 50k cells per well to yield 100k cells after 21 hours (doubling time of HCTs). Cells were then treated with either 50μM cisplatin or DMF in DMEM media for 12 hours. At 12 hours, CellTiter-Glo Reagent was added to each well, following the CellTiter-Glo Luminescent Viability Assay. Luminescence was then measured, averaging 5 wells for each condition.

### In silico modeling

We developed a simplified model of drug-target interactions in the presence of a condensate. The relevant species are the drug (D), target (T), and the drug-target complex (D-T). We assume there are only 2-types of phases, the bulk/dilute nuclear phase (n) and the condensate phase (c), which is present with volume fraction  $f = V_{condensate}/V_{nucleus}$ . At equilibrium, the following partitioning conditions are obeyed:

$$\frac{[D]_c}{[D]_n} = p_D; \frac{[T]_c}{[T]_n} = p_T;$$

where  $p_D, p_T$  are the partition coefficients of the drug and target.  $[D]_c$  represents the concentration of species D in condensate phase (and similarly for other components/phases). In this model, the drug and target complex with phase-independent disassociation constant of  $K_D$ .



$$K_D = \frac{[D][T]}{[D - T]}$$

To solve for equilibrium concentrations of various species, which are present at overall levels  $[D]_0, [T]_0$ , we write down the species balance as:

$$f([D]_c + [D - T]_c) + (1 - f)([D]_n + [D - T]_n) = [D]_0$$

$$f([T]_c + [D - T]_c) + (1 - f)([T]_n + [D - T]_n) = [DT]_0$$

We solve these 6 concentrations with 2-equations and 4 constraints (2 from partitioning and 2 from reaction equilibria). In Fig S31, the fraction of bound target is defined as:

$$Fraction_{bound, c} = \frac{[D - T]_c}{[D]_c + [T]_c}$$

A similar expression is used for the fraction of bound target in the nuclear (bulk or dilute) phase.

In case of controls plotted, we plot fraction when there is only 1 phase (f=0).

### Generation and analysis of MCF7 mEGFP-MED1 cells

To generate MCF7 mEGFP-MED1 cells, a lentiviral construct containing the full length MED1 with a N-terminal mEGFP fusion connected by a 10 amino acid GS linker was cloned, containing

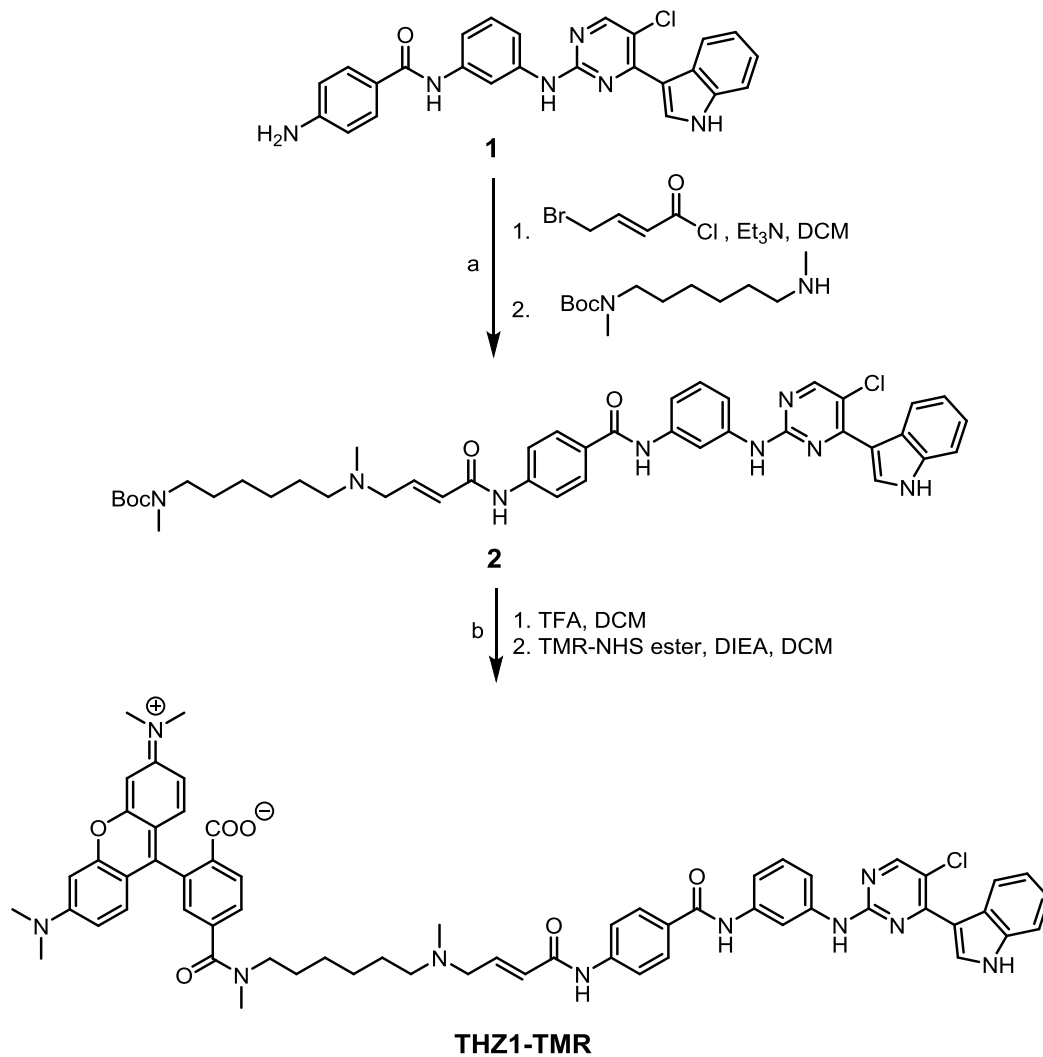
a puromycin selection marker. Lentiviral particles were generated in HEK293T cells. 250,000 MCF7 cells were plated in one well of a 6 well plate and viral supernatant was added. 48 hours later puromycin was added at 1 $\mu$ g/mL for 5 days for selection.

For live-cell FRAP experiments, the tagged MED1-mEGFP MCF7 cells were plated on Poly-L-Ornithine coated glass-bottom tissue culture plate. 20 pulses of laser at a 50 $\mu$ s dwell time were applied to the array, and recovery was imaged on an Andor microscope every 1 s for the indicated time periods. Quantification was performed in FIJI. The instrument background was subtracted from the average signal intensity in the bleached puncta then divided by the instrument background subtracted from a control puncta. These values were plotted every second, and a best fit line with 95% confidence intervals was calculated. For observing fusions of MED1-GFP foci, MED1-mEGFP MCF7 cells were grown for 3 days in estrogen-free conditions then plated on glass-bottomed plates. 15 minutes prior to imaging, cells were treated with 100nM estrogen and placed on the Andor confocal microscope and imaged at 150x for 4 minutes. Images were post-processed in FIJI. Fluorescent intensity calculations were made in FIJI.

### Chemistry

Unless otherwise noted, reagents and solvents were obtained from commercial suppliers and were used without further purification. Mass spectra were obtained on a Waters Micromass ZQ instrument. Preparative HPLC was performed on a Waters Sunfire C18 column (19 mm  $\times$  50 mm, 5  $\mu$ M) using a gradient of 15–95% methanol in water containing 0.05% trifluoroacetic acid (TFA) over 22 min (28 min run time) at a flow rate of 20 mL/min.

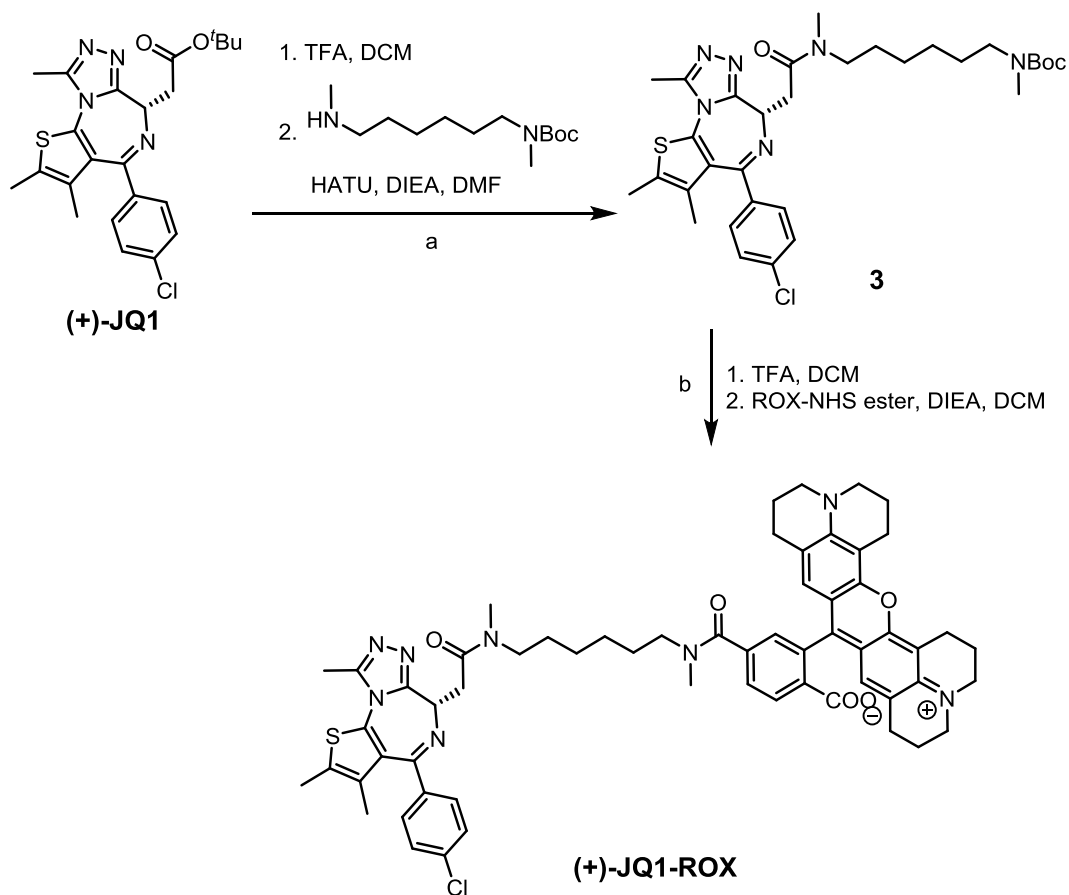
Scheme 1: Synthesis of THZ1-TMR



Reagents and conditions: (a) (*E*)-4-bromobut-2-enoyl chloride, triethyl amine, DCM, 0 °C~r.t., then *tert*-butyl methyl(6-(methylamino)hexyl)carbamate, r.t.~50 °C; (b) trifluoroacetic acid, DCM, r.t., then TMR-NHS ester, diisopropylethyl amine, DCM, r.t.~40 °C *tert*-butyl *E*-(6-(((4-(((3-((5-chloro-4-(1H-indol-3-yl)pyrimidin-2-yl)amino)phenyl) carbamoyl)phenyl)amino)-4-oxobut-2-en-1-yl)(methyl)amino)hexyl)(methyl)carbamate (2). To a solution of 1 (20 mg, 0.044 mmol, prepared according to patent WO2014/63068) and triethyl amine (29 mg, 0.27 mmol) in 0.8 mL DCM was added (*E*)-4-bromobut-2-enoyl chloride (0.24 mL, 0.2 M in DCM). The solution was stirred for 6 hours. Then *tert*-butyl methyl(6-(methylamino)hexyl)carbamate (13 mg, 0.052

mmol) in 0.4 mL DCM was added. The mixture was warmed to 50 °C and kept overnight. The mixture was concentrated in vacuo, then purified by preparative HPLC to provide intermediate 2 (6 mg, 19%). LC/MS (ESI)  $m/z = 765$  (M + H)<sup>+</sup>. (*E*)-4-((6-((4-((4-((3-((5-chloro-4-(1H-indol-3-yl)pyrimidin-2-yl)amino)phenyl)carbamoyl)phenyl)amino)-4-oxobut-2-en-1-yl)(methyl)amino)hexyl)(methyl)carbamoyl)-2-(6-(dimethylamino)-3-(dimethyliminio)-3H-xanthen-9-yl)benzoate (THZ1-TMR). To a solution of 2 (6 mg, 0.0078 mmol) in 0.5 mL DCM was added 0.1 mL TFA. The resultant solution was stirred at room temperature for 1 h, and then concentrated in vacuo to obtain free amine as TFA salt, which was dissolved in 0.5 mL DCM again. To this solution DIEA (5mg, 0.039 mmol) and TMR-NHS ester (5 mg, 0.0094 mmol) were added in sequence. The mixture was warmed to 40 °C and kept overnight. The mixture was concentrated in vacuo, then purified by preparative HPLC to provide THZ1-TMR (2 mg, 23%). LC/MS (ESI)  $m/z = 1077$  (M + H)<sup>+</sup>.

Scheme 2: Synthesis of (+)-JQ1-ROX



Reagents and conditions: (a) trifluoroacetic acid, DCM, r.t., then *tert*-butyl methyl(6-(methylamino)hexyl)carbamate, 1-[bis(dimethylamino)methylene]-1H-1,2,3-triazolo[4,5-b]pyridinium 3-oxid hexafluorophosphate, diisopropylethyl amine, DMF, r.t.; (b) trifluoroacetic acid, DCM, r.t., then ROX-NHS ester, diisopropylethyl amine, DCM, r.t.~40 °C *tert*-butyl (*S*)-(6-(2-(4-(4-chlorophenyl)-2,3,9-trimethyl-6H-thieno[3,2-*f*][1,2,4]triazolo[4,3-*a*][1,4]diazepin-6-yl)-N-methylacetamido)hexyl)(methyl)carbamate (**3**) To a solution of (+)-JQ1 (25 mg, 0.055 mmol) in 2 mL DCM was added 0.4 mL TFA. The resultant solution was stirred at room temperature for 1 h, and then concentrated in vacuo to obtain free amine as TFA salt, which was dissolved in 0.8 mL DMF. To this solution was added *tert*-butyl methyl(6-(methylamino)hexyl)carbamate (16 mg, 0.065 mmol) in 0.5 mL DMF, DIEA (35mg, 0.28 mmol) and HATU (24 mg, 0.064 mmol) in

sequence. The mixture was stirred at r.t. for 6 hours. Then purified by preparative HPLC to provide intermediate 3 (15 mg, 43%). LC/MS (ESI)  $m/z = 627 (M + H)^+$ .

(+)JQ1-ROX. To a solution of 3 (15 mg, 0.024 mmol) in 2 mL DCM was added 0.4 mL TFA. The resultant solution was stirred at room temperature for 1 h, and then concentrated in vacuo to obtain free amine as TFA salt, which was dissolved in 1 mL DCM again. To this solution DIEA (16mg, 0.12 mmol) and ROX-NHS ester (13mg, 0.021 mmol) were added in sequence. The mixture was warmed to 40°C and kept overnight. The mixture was concentrated in vacuo, then purified by preparative HPLC to provide (+)JQ1-ROX (6 mg, 28), LC/MS (ESI)  $m/z = 1043 (M + H)^+$ .

#### Immunofluorescence with DNA FISH

MCF7 cells were grown in estrogen-free DMEM for 3 days on Poly-L-ornithine coated coverslips in 24 well plates at an initial seeding density of 50,000 cells per well. Cells were then treated with vehicle, 10nM estradiol, or 10nM estradiol and 5uM 4-hydroxytamoxifen for 45 minutes. HCT116 cells were treated with 1µM JQ1 for 24 hours, followed by cell permeabilization (10min at 37°C with the solution of tx100 in PBS at 1:1000 in media) and subsequently DMF or 50µM Cisplatin for 6 hours.

Cells on cover slips were then fixed in 4% paraformaldehyde. Immunofluorescence was performed as described above. After incubating the cells with the secondary antibodies, cells were washed three times in PBS for 5min at RT, fixed with 4% PFA in PBS for 10min and washed three times in PBS. Cells were incubated in 70% ethanol, 85% ethanol and then 100% ethanol for 1 minute at RT. Probe hybridization mixture was made mixing 7µL of FISH Hybridization Buffer (Agilent G9400A), 1µL of FISH probes (SureFISH 8q24.21 MYC 294kb G101211R-8) and 2µL of water.

5µL of mixture was added on a slide and coverslip was placed on top (cell-side toward the hybridization mixture). Coverslip was sealed using rubber cement. Once rubber cement solidified, genomic DNA and probes were denatured at 78°C for 5 minutes and slides were incubated at 16°C in the dark O/N. The coverslip was removed from slide and incubated in pre-warmed Wash Buffer 1 (Agilent, G9401A) at 73°C for 2 minutes and in Wash Buffer 2 (Agilent, G9402A) for 1 minute at RT. Slides were air dried and nuclei were stained in 20µm/mL Hoechst 33258 (Life Technologies, H3569) in PBS for 5 minutes at RT. Coverslips were washed three times in PBS, followed by mounting the coverslip onto glass slides, sealing, imaging, and post-processing as described above.

#### RT-qPCR

MCF7 cells were estrogen deprived for 3 days then stimulated with either 10nM estrogen or 10nM estrogen and 5µM 4-hydroxytamoxifen for 24 hours. RNA was isolated by AllPrep Kit (Qiagen 80204) followed by cDNA synthesis using High-Capacity cDNA Reverse Transcription Kit (Applied Biosystems 4368814). qPCR was performed in biological and technical triplicate using Power SYBR Green mix (Life Technologies #4367659) on a QuantStudio 6 System (Life Technologies). The following oligos was used in the qPCR; Myc fwd AACCTCACAACCTTGGCTGA, MYC rev TTCTTTTATGCCCAAAGTCCAA, GAPDH fwd TGCACCACCAACTGCTTAGC, GAPDH rev GGCATGGACTGTGGTCATGAG. Fold change was calculated and *MYC* expression values were normalized to *GAPDH* expression.

#### LAC binding assay

Constructs were assembled by NEB HIFI cloning in pSV2 mammalian expression vector containing an SV40 promoter driving expression of a mCherry-LacI fusion protein. The intrinsically disordered region of MED1, HP1 $\alpha$ , or the activation domain of *ESR1* was fused by the c-terminus to this recombinant protein, joined by the linker sequence GAPGSAGSAAGGSG. For experiments comparing FLTX1 enrichment at the array, U2OS-Lac cells were plated onto chambered coverglass (1.5 Borosilicate Glass, Nunc Lab-Tek, 155409) and transfected with either MED1 IDR or HP1 $\alpha$  constructs with lipofectamine 3000 (Thermofisher L3000015). After 24 hours, cells were treated with either 1 $\mu$ M FLTX1 or vehicle (DMF). After 30 minutes, cells were imaged on the Zeiss LSM 880 confocal microscope with Airyscan detector with 63x objective at 37°C. For experiments with high MED1, cells grown in DMEM were plated on glass coverslips and transfected using lipofectamine 3000 (Thermofisher L3000015). A construct with a mammalian expression vector containing a PGK promoter driving the expression of MED1 fused to GFP was co-transfected in high MED1 conditions. 24 hours after transfection, cells were treated for 45 minutes with 4-Hydroxytamoxifen (Sigma-Aldrich H7904) reconstituted in DMSO. Following treatment, cells were fixed and immunofluorescence was performed with a MED1 antibody as described above. Cells were then imaged using the RPI Spinning Disk confocal microscope with a 100x objective. Images were post-processed in FIJI.

For analysis of Lac array data comparing MED1 or HP1 $\alpha$  tethered, a region of interest was called using the signal in the Lac array (561 channel). The average fluorescent signal for FLTX1 (488 channel) was then measured in the region of interest and divided by the average fluorescence in the region of interest at the Lac array. This value was then divided in the drug treated condition by the vehicle treated condition and all values were normalized to the HP1 $\alpha$  condition. For analysis

of Lac array data for MED1 overexpression, enrichment was calculated by dividing the average fluorescent signal for MED1 immunofluorescence at the region of interest, defined by the ER tethered at the lac array, by MED1 immunofluorescence signal at a random nuclear region. Enrichment of MED1 was plotted over each concentration of tamoxifen in wildtype or high MED1 conditions.

### Western blot

Cells were lysed in Cell Lytic M (Sigma-Aldrich C2978) with protease inhibitors (Roche, 11697498001). Lysate was run on a 3%–8% Tris-acetate gel or 10% Bis-Tris gel or 3-8% Bis-Tris gels at 80 V for ~2 hrs, followed by 120 V until dye front reached the end of the gel. Protein was then wet transferred to a 0.45  $\mu$ m PVDF membrane (Millipore, IPVH00010) in ice-cold transfer buffer (25 mM Tris, 192 mM glycine, 10% methanol) at 300 mA for 2 hours at 4°C. After transfer the membrane was blocked with 5% non-fat milk in TBS for 1 hour at room temperature, shaking. Membrane was then incubated with 1:1,000 of the indicated antibody (ER ab32063, MED1 ab64965) diluted in 5% non-fat milk in TBST and incubated overnight at 4°C, with shaking. In the morning, the membrane was washed three times with TBST for 5 minutes at room temperature shaking for each wash. Membrane was incubated with 1:5,000 secondary antibodies for 1 hr at RT and washed three times in TBST for 5 minutes. Membranes were developed with ECL substrate (Thermo Scientific, 34080) and imaged using a CCD camera or exposed using film or with high sensitivity ECL. Quantification of western blot was performed using BioRad image lab.

**Fig. S1.**

Figure S1

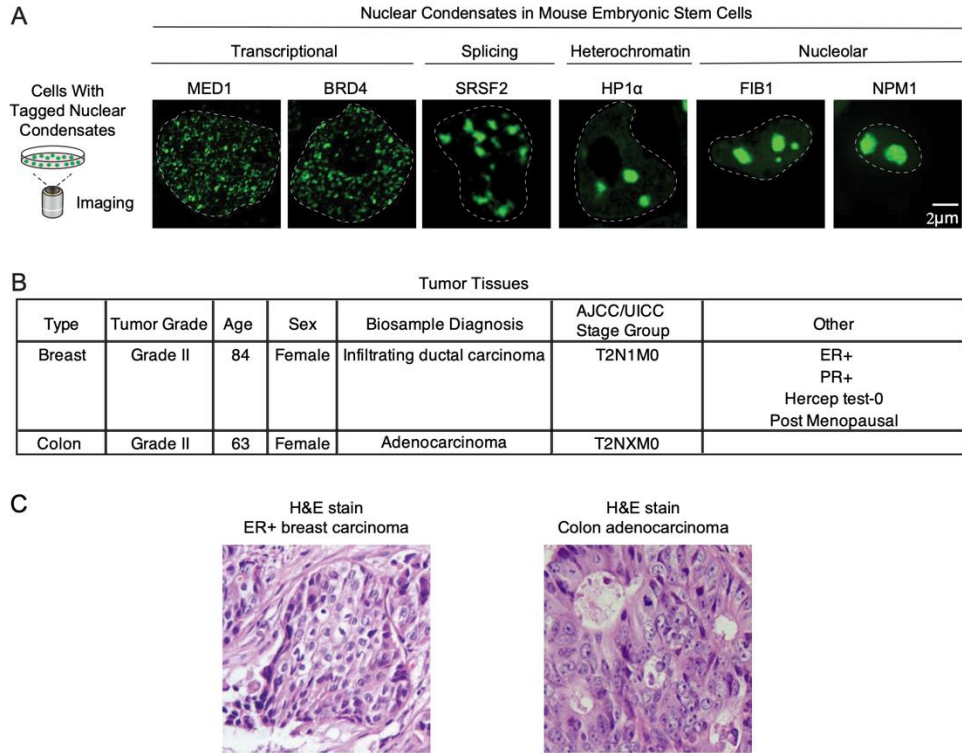


Figure S1. Nuclear condensates in cell lines and human tumor tissue. (A) Mouse embryonic stem cells expressing either endogenously mEGFP-tagged proteins (MED1, BRD4, SRSF2), mCherry-tagged proteins (HP1 $\alpha$ ) or transfected with constructs expressing GFP-tagged proteins (NPM1, FIB1) were imaged by confocal fluorescent microscopy. (B) Clinical data from biopsied breast and colon cancer specimen. (C) H&E staining of ER positive breast carcinoma and colon adenocarcinoma.

**Fig. S2.**

Figure S2

**A**

Percent Nuclear Volume of Nuclear condensates

	Transcriptional		Splicing	Heterochromatin	Nucleolar		Total
	MED1	BRD4	SRSF2	HP1 $\alpha$	FIB1	NPM1	
Normal Breast Tissue	2.1 +/- 6.9%	1.8 +/- 2.0%	7.3 +/- 0.2%	2.8 +/- 1.2%	11 +/- 1.4%	8.3 +/- 1.2%	33.3%
Malignant Breast Tissue	2.8 +/- 2.0%	1.9 +/- 3.3%	6.9 +/- 4.3%	2.9 +/- 3.3%	7.6 +/- 2.3%	5.8 +/- 3.3%	27.9%
Normal Colon Tissue	4.1 +/- 1.0%	10 +/- 3.7%	4.9 +/- 1.6%	7.9 +/- 3.7%	11 +/- 9.9%	6.6 +/- 1.5%	44.5%
Malignant Colon Tissue	2.6 +/- 1.5%	2.0 +/- 0.8%	6.1 +/- 2.1%	8.8 +/- 7.2%	13 +/- 7.3%	10 +/- 11%	42.5%

**B**

Average Volume of Nuclear condensates

	Transcriptional		Splicing	Heterochromatin	Nucleolar	
	MED1	BRD4	SRSF2	HP1 $\alpha$	FIB1	NPM1
Normal Breast Tissue	0.021 +/- 0.018	0.026 +/- 0.013	0.018 +/- 0.005	0.052 +/- 0.028	0.059 +/- NA	2.653 +/- 2.209
Malignant Breast Tissue	0.015 +/- 0.003	0.028 +/- 0.005	0.037 +/- 0.026	0.018 +/- 0.009	0.143 +/- 0.119	0.816 +/- 0.692
Normal Colon Tissue	0.034 +/- 0.008	0.084 +/- 0.055	0.039 +/- 0.009	0.048 +/- 0.015	0.762 +/- 0.957	0.950 +/- 0.861
Malignant Colon Tissue	0.040 +/- 0.017	0.023 +/- 0.004	0.046 +/- 0.007	0.038 +/- 0.023	0.927 +/- 1.521	0.431 +/- 0.270

**C**

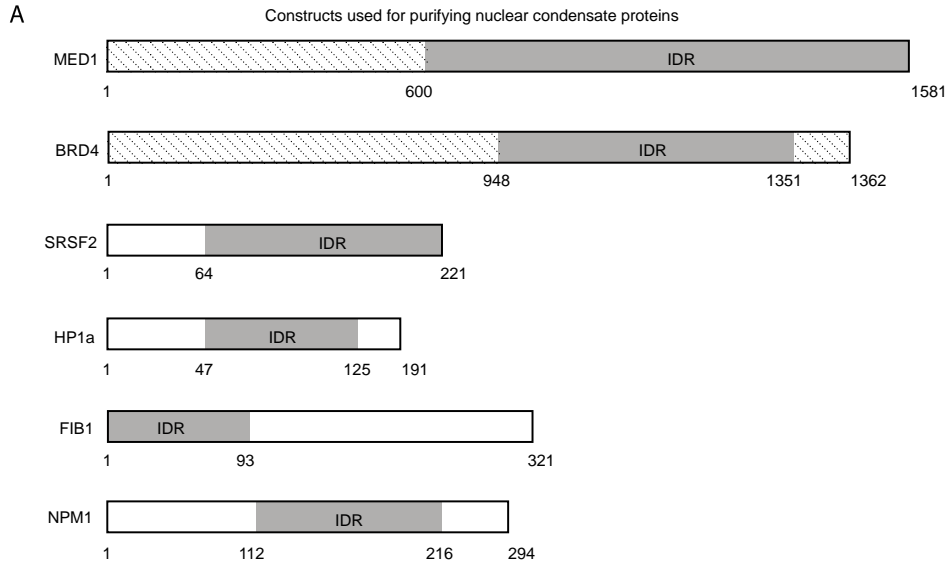
Average Number of Nuclear condensates

	Transcriptional		Splicing	Heterochromatin	Nucleolar	
	MED1	BRD4	SRSF2	HP1 $\alpha$	FIB1	NPM1
Normal Breast Tissue	93 +/- 54.9	53 +/- 20.9	37 +/- 20.5	55 +/- 57.3	18 +/- NA	4 +/- 5.2
Malignant Breast Tissue	78 +/- 41.1	72 +/- 28.0	32 +/- 16.1	133 +/- 81.0	21 +/- 6.4	8 +/- 6.0
Normal Colon Tissue	60 +/- 7.9	15 +/- 8.1	47 +/- 20.1	74 +/- 49.2	10 +/- 10.4	5 +/- 2.9
Malignant Colon Tissue	24 +/- 12.9	66 +/- 19.3	47 +/- 28.9	42 +/- 18.9	13 +/- 14.6	11 +/- 7.4

Figure S2. Volume and number of nuclear condensates in normal and tumor tissue. (A) Volume of nuclear condensates in normal and malignant breast tissue (upper) and in normal and malignant colon tissue (lower). Values indicate percent nuclear volume and standard deviation. There were no significant differences between the individual nuclear condensates in normal and malignant states. (B) Table showing average volume of nuclear condensates in normal and malignant tissue. (C) Table showing average number of nuclear condensates in normal and malignant tissue.

**Fig. S3.**

Figure S3



**B**

	Aromatic Amino Acid Analysis							
	Full-length Protein				IDR			
	F	W	Y	Total	F	W	Y	Total
MED1	40	4	26	70	19	1	10	30
BRD4	25	5	18	48	10	1	2	13
FIB1	13	1	7	21	6	0	0	6
HP1 $\alpha$	6	4	5	15	3	1	1	5
SRSF2	4	0	9	13	0	0	4	4
NPM1	7	2	4	13	2	0	0	2

	Basic/Acidic Patch Analysis			
	Total		IDR	
	CIE+	CIE-	CIE+	CIE-
MED1	11	10	7	3
BRD4	11	9	3	3
FIB1	3	0	2	0
HP1 $\alpha$	4	4	3	1
SRSF2	4	2	4	2
NPM1	3	4	3	2

Figure S3. Nuclear condensate forming proteins. (A) Schematic representation of constructs used for purifying nuclear condensate proteins. The IDR (intrinsically disordered region) alone was used for MED1 and BRD4 proteins and the full length was used for HP1 $\alpha$ , SRSF2, NPM1, and FIB1 proteins. (B) (Upper) Number of hydrophobic amino acids Phenylalanine (F), Tryptophan

(W), and Tyrosine (Y) in the IDR and full-length protein. MED1 IDR has the highest number of hydrophobic residues. (Lower) Table of Positive Charged Interaction Elements (CIE+) and Negative Charged Interaction Elements (CIE-) of the IDR or full length nuclear condensate protein (63). These results indicate that MED1 protein might participate in interactions governed by the pi-system.

**Fig. S4.**

Figure S4

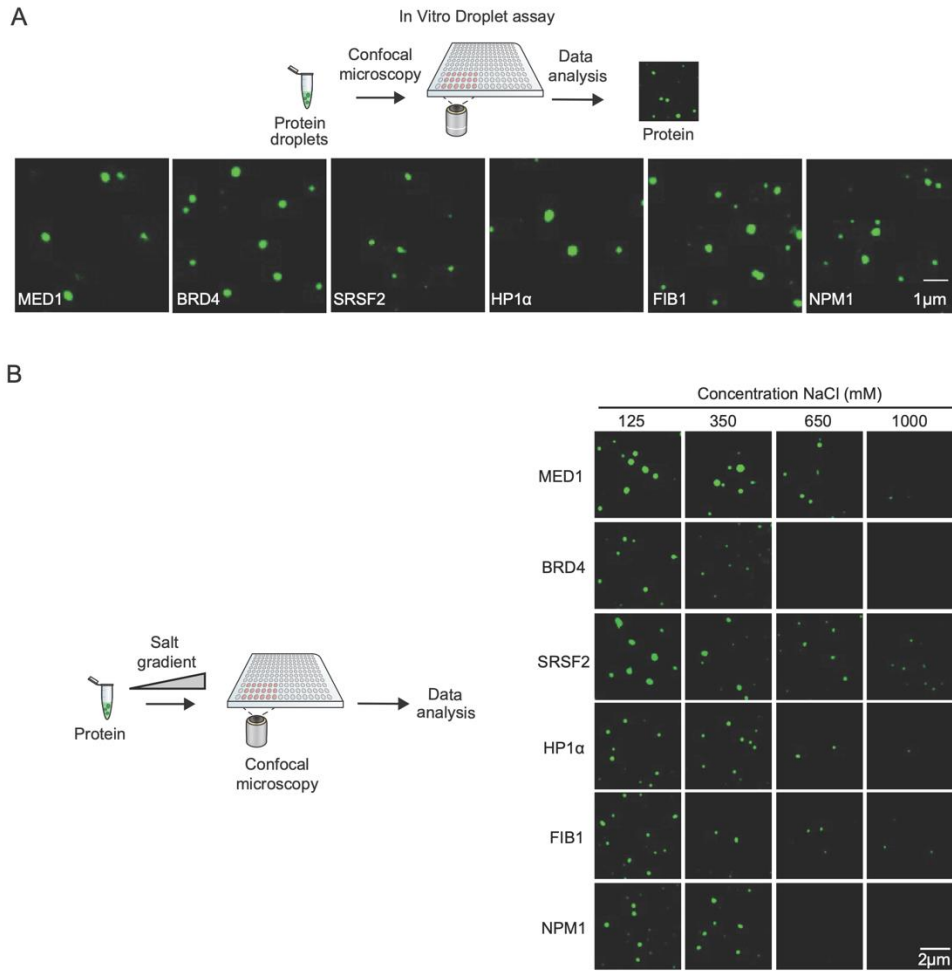
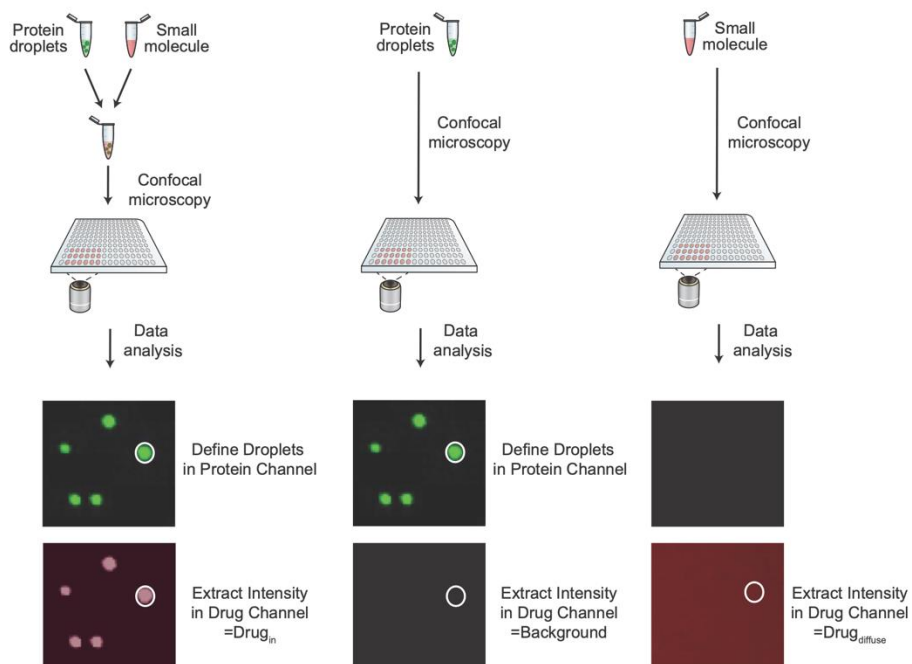


Figure S4. In vitro droplets of condensate forming proteins. (A) Confocal microscopy of in vitro droplet formation assays of the indicated GFP-tagged protein in 125mM NaCl and 10% PEG. MED1 and BRD4 proteins are the IDR portion only. (B) Confocal microscopy images of MED1, BRD4, SRSF2, HP1 $\alpha$ , FIB1, and NPM1 nuclear condensates at the indicated concentration of salt (125mM, 350mM, 650mM, 1000mM NaCl), experiments were performed with 10 $\mu$ M protein in 10% PEG.

**Fig. S5.**

Figure S5



$$\text{Enrichment Ratio} = \frac{\text{Drug}_{in} - \text{Background}}{\text{Drug}_{diffuse}}$$

Figure S5. Schematic representation of enrichment ratio calculations. Droplets are defined in the protein channel and maximum intensity of drug is measured in that area to obtain  $\text{drug}_{in}$  (left panel), background is measured in the drug channel in areas defined by the protein channel in an in vitro droplet reaction containing protein but no drug (middle panel), and  $\text{drug}_{diffuse}$  intensity is measured in a droplet reaction without the protein (right panel).

**Fig. S6.**

**Figure S6**

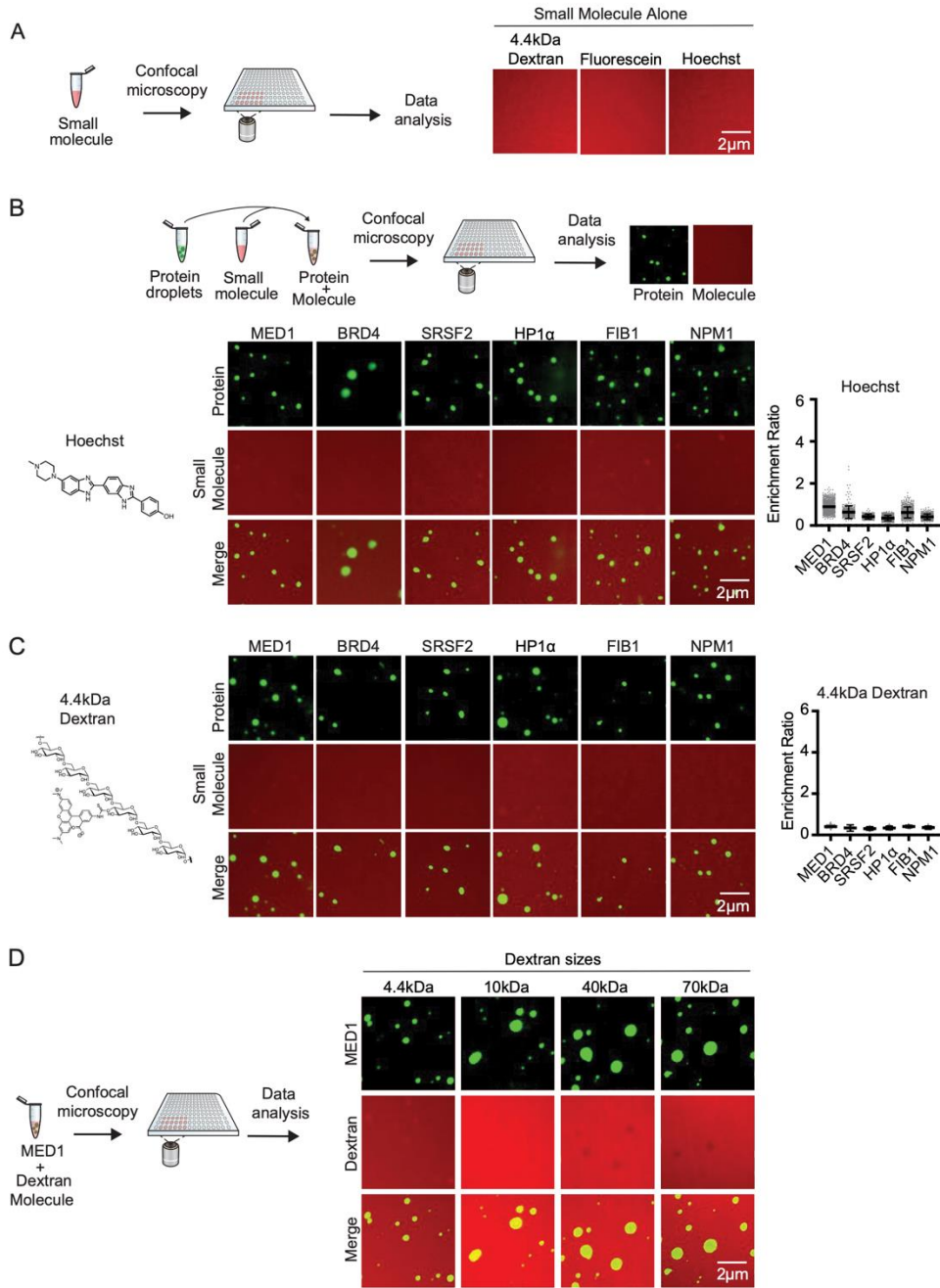


Figure S6. Small molecule partitioning in nuclear condensates. (A) Confocal microscopy of in vitro droplet formation assays of the indicated small molecule alone (4.4kDa dextran, fluorescein, and hoechst) without any protein added to the reaction. All small molecules alone show a diffuse

fluorescent signal indicating that the molecule alone does not form droplets. (B-C) Confocal microscopy images showing the behavior of hoechst (B) and 4.4kDa dextran (C) relative to six nuclear condensates formed in vitro, in 125mM NaCl and 10% PEG. Quantification shown to the right, error bars represent SEM. Both hoechst and dextran diffuse freely through the condensates tested without being excluded or concentrated. Schematic of the assay shown at top. (D) Confocal microscopy images of fluorescently-labeled 4.4kDa, 10kDa, 40kDa, and 70kDa dextran in MED1 condensates. Experiments were performed with 10 $\mu$ M protein and 0.1mg/ml TRITC-labeled dextran, in 125mM salt and 16% ficoll. Dextran of smaller sizes (4.4kDa and 10kDa) are able to freely diffuse through the condensates while larger sizes of dextran (40kDa and 70kDa) are partially excluded from MED1 condensates. This indicates that the effective pore sizes of the condensates studied is at least 10kDa (65).

Fig. S7.

Figure S7

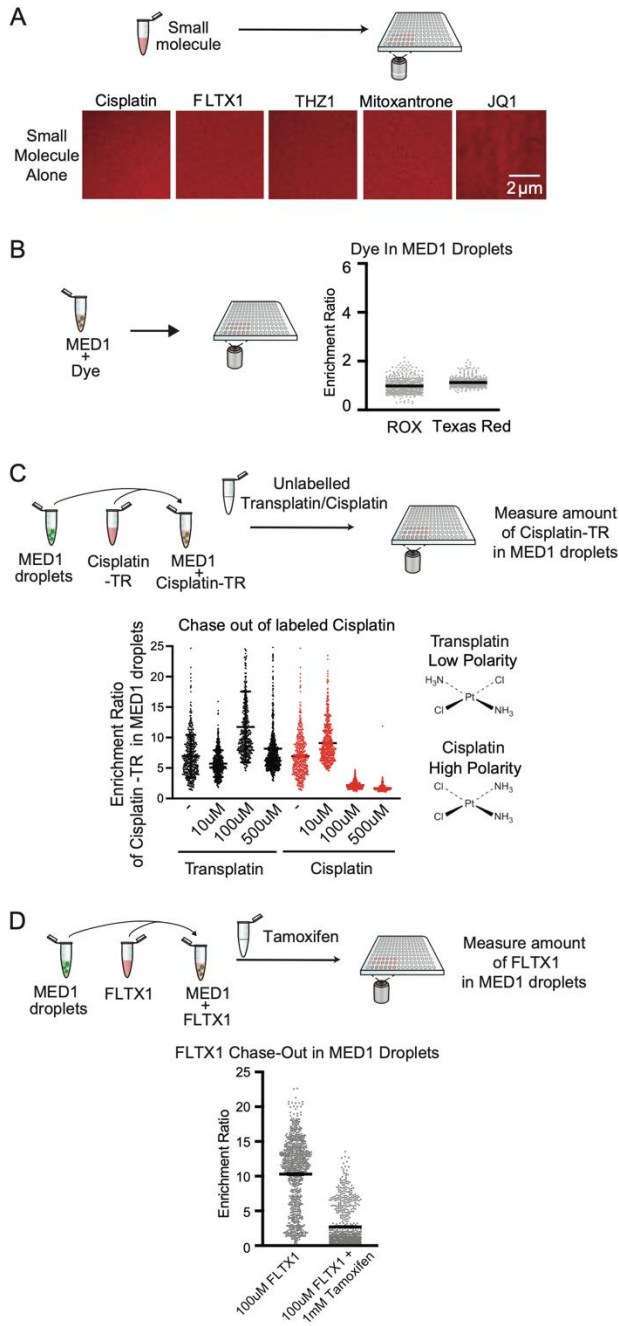


Figure S7. Properties of small molecule drugs, not their fluorescent moiety, govern partitioning into condensates. (A) Confocal microscopy of in vitro droplet formation assays of the indicated small molecule drug alone (cisplatin, FLTX1, THZ1, mitoxantrone, and JQ1) without any protein added

to the reaction. All small molecule drugs alone show a diffuse fluorescent signal indicating that the molecules alone do not form droplets. (B) ROX and Texas Red enrichment in MED1 droplets formed in 125mM NaCl and 10% PEG measured by confocal microscopy. Neither of the two dyes used to visualize drugs were enriched in MED1 condensates. (C) Schematic of in vitro droplet drug chase out experiment. Labeled cisplatin is added to MED1 droplets to form MED1 droplets concentrated with cisplatin-TR. Unlabeled transplatin or unlabeled cisplatin is added to the droplet mixture and the amount of labeled cisplatin-TR remaining in the droplet is measured after chase out. Transplatin, a clinically ineffective trans-isomer of cisplatin, is not able to chase out cisplatin-TR, while high concentrations of unlabeled cisplatin is able to chase out cisplatin-TR. (D) Schematic of in vitro droplet drug chase out experiment. Graph showing FLTX1 enrichment in MED1 droplets upon tamoxifen addition measured by confocal microscopy. Tamoxifen was able to chase-out FLTX1 from MED1 droplets. All error bars shown represent SEM.

**Fig. S8.**

Figure S8

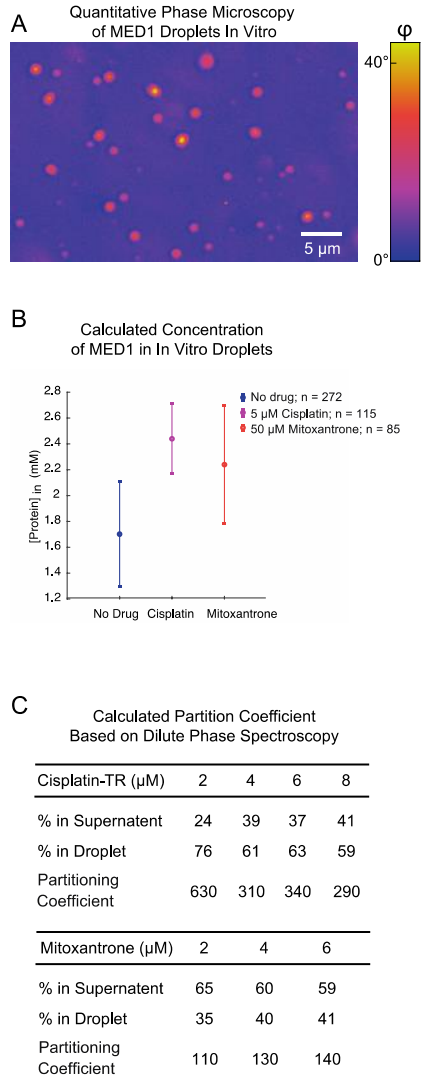


Figure S8. Small molecule drugs can be concentrated into MED1 condensates by 100-folds. (A) Quantitative phase microscopy of MED1 droplets formed in 125 mM NaCl and 10% PEG. Colorbar indicates optical phase delay,  $\phi$ , in degrees. From phase images, we calculate the average MED1 concentration in individual condensates. (B) Graph showing MED1 concentration in in vitro droplets upon the addition of no drug, 5  $\mu\text{M}$  cisplatin or 50  $\mu\text{M}$  mitoxantrone. Datapoints are

population averages ( $n = 272, 115$  and  $85$  individual condensates for each condition). Error bars denote standard deviation. (C) Varying concentration of cisplatin or Mitoxantrone was added to MED1 droplets and the concentration of drug remaining in solution was measured by uv-spectroscopy. Combining the spectroscopy measurements with an estimate of the total volume of the MED1 condensate phase obtained from the measurements in (B), we estimate the partition ratio of cisplatin to be up to 600-fold and the partitioning ratio of Mitoxantrone to be approximately 100-fold.

**Fig. S9.**

Figure S9

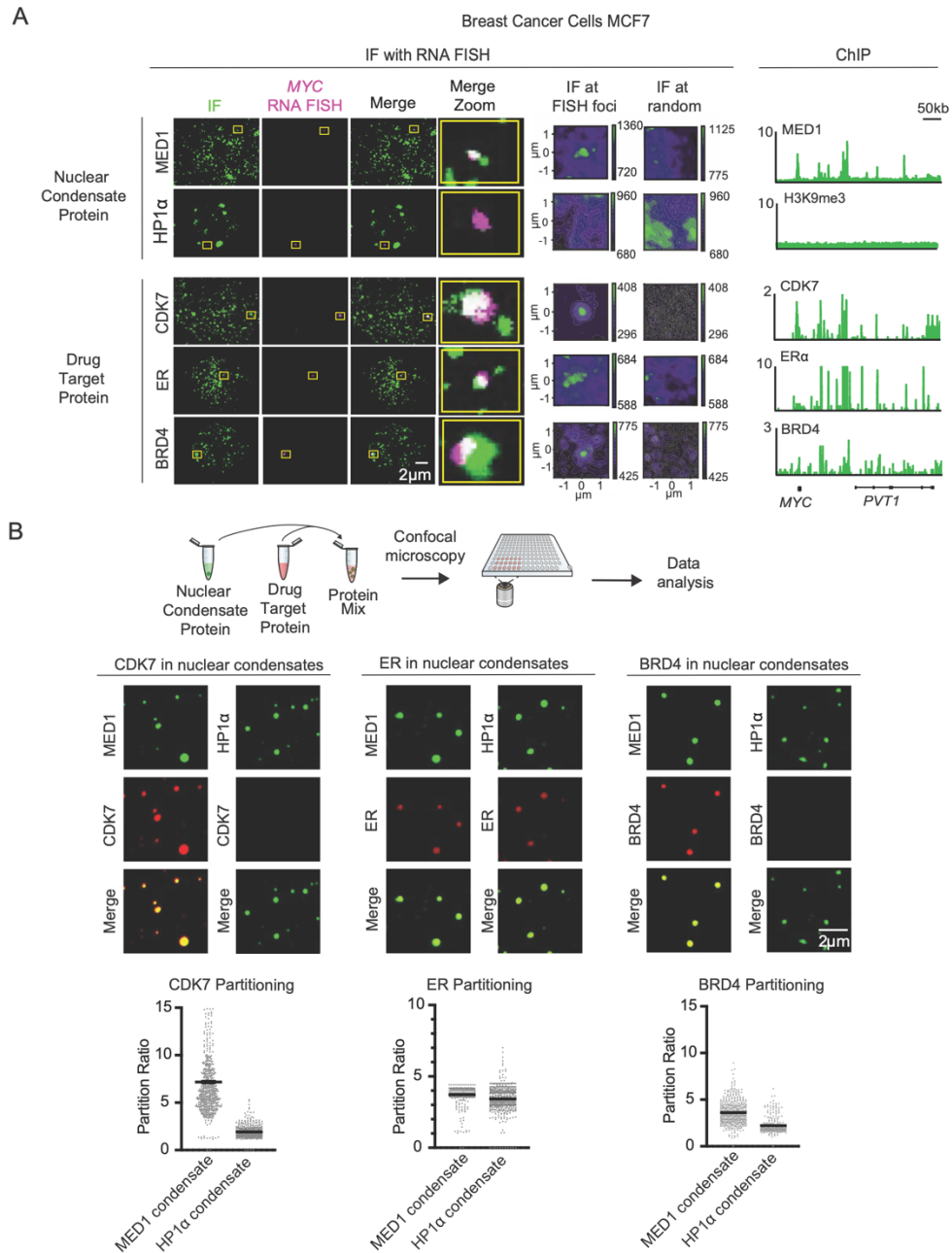


Figure S9. Association of drug targets with transcriptional condensates. (A) Immunofluorescence of MED1, HP1 $\alpha$ , CDK7, ER, and BRD4 together with MYC RNA FISH. Consistent with the finding that MED1, a marker of transcriptional condensates, is present in puncta at the MYC

oncogene, CDK7, ER, and BRD4 are also found in puncta at *MYC*. These results mirror those obtained by ChIP-Seq at this locus. In contrast, signal for HP1 $\alpha$ , a marker of heterochromatin condensates, is not found at *MYC*. Average and random image analysis shown to the right. (B) (Top) Schematic of in vitro droplet assay showing mixing of nuclear condensate protein (MED1 or HP1 $\alpha$ ) with various drug target proteins (CDK7, ER, or BRD4), with partitioning into the nuclear condensate measured by confocal microscopy. (Middle) In vitro droplet assays with MED1, ER, HP1 $\alpha$  and BRD4 at 10 $\mu$ M, CDK7 at 200nM. Droplets are formed in 125mM NaCl, 10% PEG and droplet formation buffer. All drug targets tested were concentrated in MED1 condensates. ER was found to be concentrated both in MED1 and HP1 $\alpha$  condensates, consistent with previous reports and its ability to associate with both co-activators and co-repressors (12, 66). (Bottom) Quantification of target protein enrichment in the indicated condensates, error bars represent SEM.

**Fig. S10.**

Figure S10

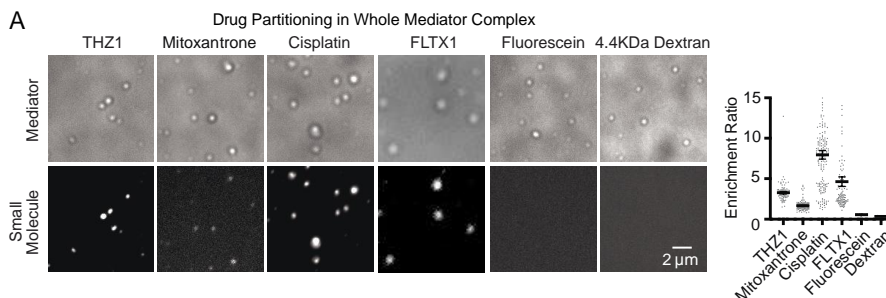


Figure S10. Partitioning behavior of various small molecule drugs in whole Mediator complex. Confocal microscopy images of drugs (THZ1, mitoxantrone, cisplatin, FLTX1, fluorescein, and 4.4kDa dextran) in whole mediator complex condensates. Mediator was imaged in brightfield while the small molecule was imaged by the channel in which it fluoresces. Experiments were performed in 10% PEG and 125mM NaCl. The partitioning behavior of various small molecule drugs into whole Mediator complex recapitulate the partitioning behavior of drugs into MED1 condensates. Quantification of enrichment shown to the right, error bars represent SEM.

**Fig. S11.**

Figure S11

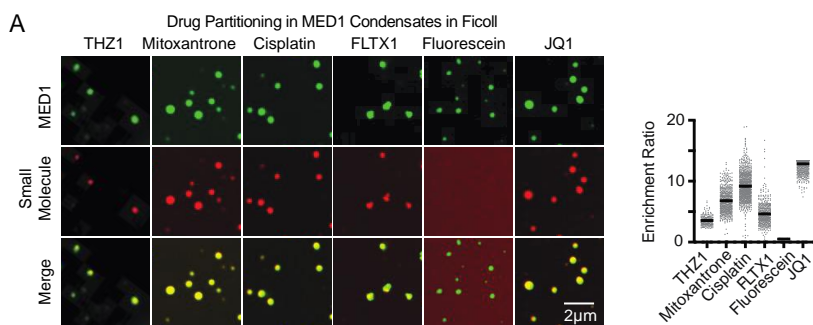


Figure S11. Partitioning behavior of various small molecule drugs into MED1 condensates formed in ficoll. Confocal microscopy images of small molecule drugs (THZ1, mitoxantrone, cisplatin, FLTX1, fluorescein, and JQ1) concentration behavior in MED1 condensates in the presence of 125mM NaCl and 20% ficoll. The partitioning behavior of small molecules are similar regardless of crowder used to form MED1 droplets. Quantification of enrichment shown to the right, error bars represent SEM.

**Fig. S12.**

Figure S12

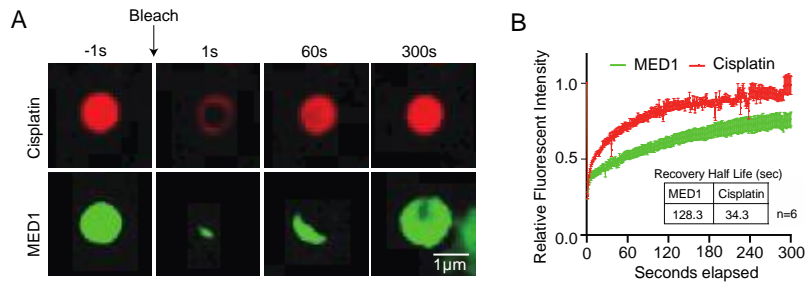


Figure S12. Cisplatin molecules are highly mobile in MED1 droplets. (A) Confocal microscopy images showing fluorescence recovery after photobleaching (FRAP) of TR-cisplatin and MED1 in condensates formed in the presence of 125mM NaCl and 10% PEG with 5µM TR-cisplatin and 10µM protein. (B) Quantification of FRAP (error bars represent SEM).

Fig. S13.

Figure S13

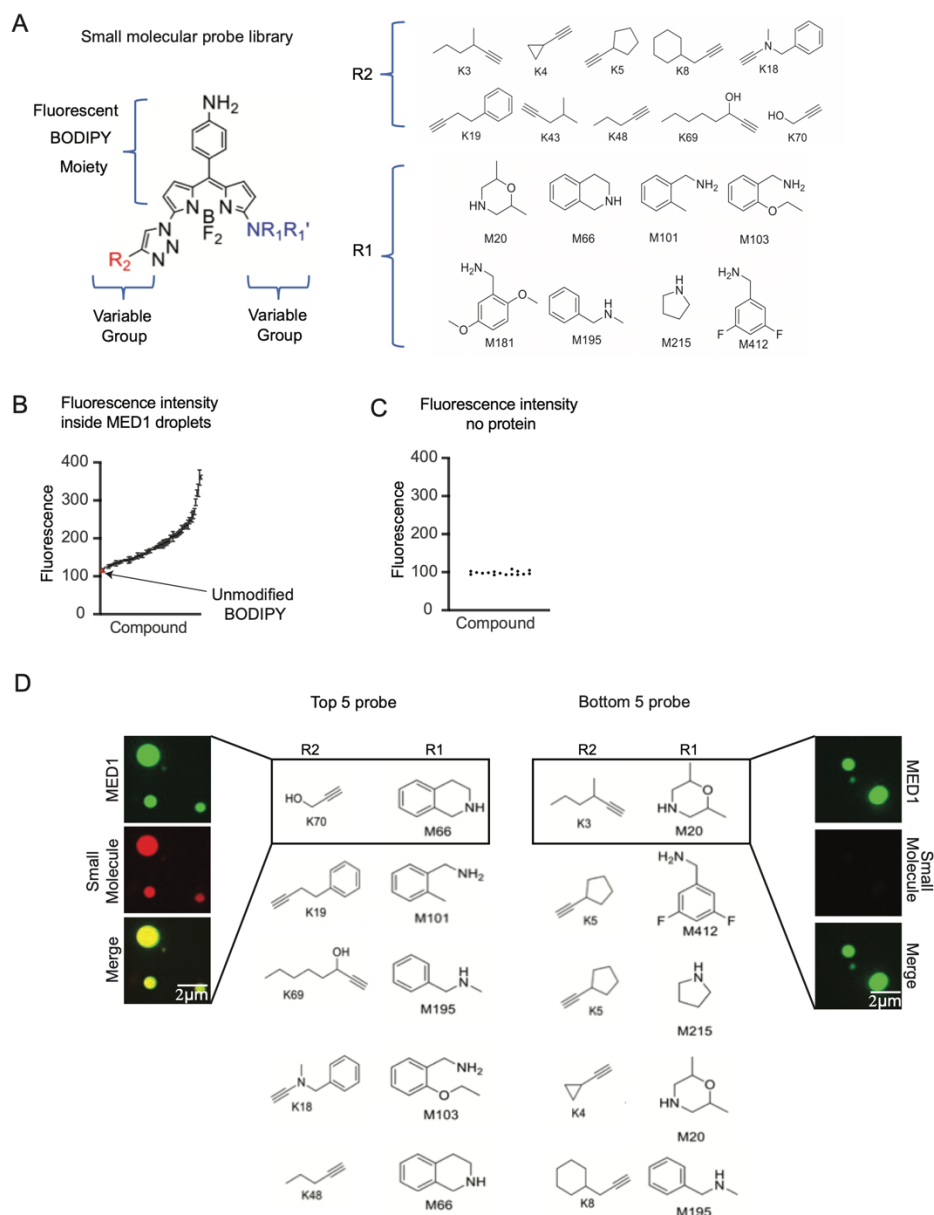


Figure S13. Specific chemical moieties govern concentration in MED1 condensates. (A) Depiction of small molecule boron-dipyrromethene (BODIPY) library. (B) Fluorescence intensity of probe library in MED1 droplets measured by confocal microscopy. Experiments were performed in 125mM NaCl and 10% PEG, with 10 $\mu$ M MED1 and 1 $\mu$ M small molecule. The fluorescence of

the BODIPY molecule alone is highlighted in red. (C) Fluorescent intensity of a random selection of 18 probes from the library without MED1 protein demonstrating they have similar fluorescent intensity. (D) Top 5 (left) and bottom 5 (right), R2 and R1 sidechains, ranked by fluorescent intensity. This screen of 81 compounds suggests that pi-system interactions mediate compound accumulation in condensates, a larger screen will further define the chemical features that mediate this phenomenon.

**Fig. S14.**

**Figure S14**

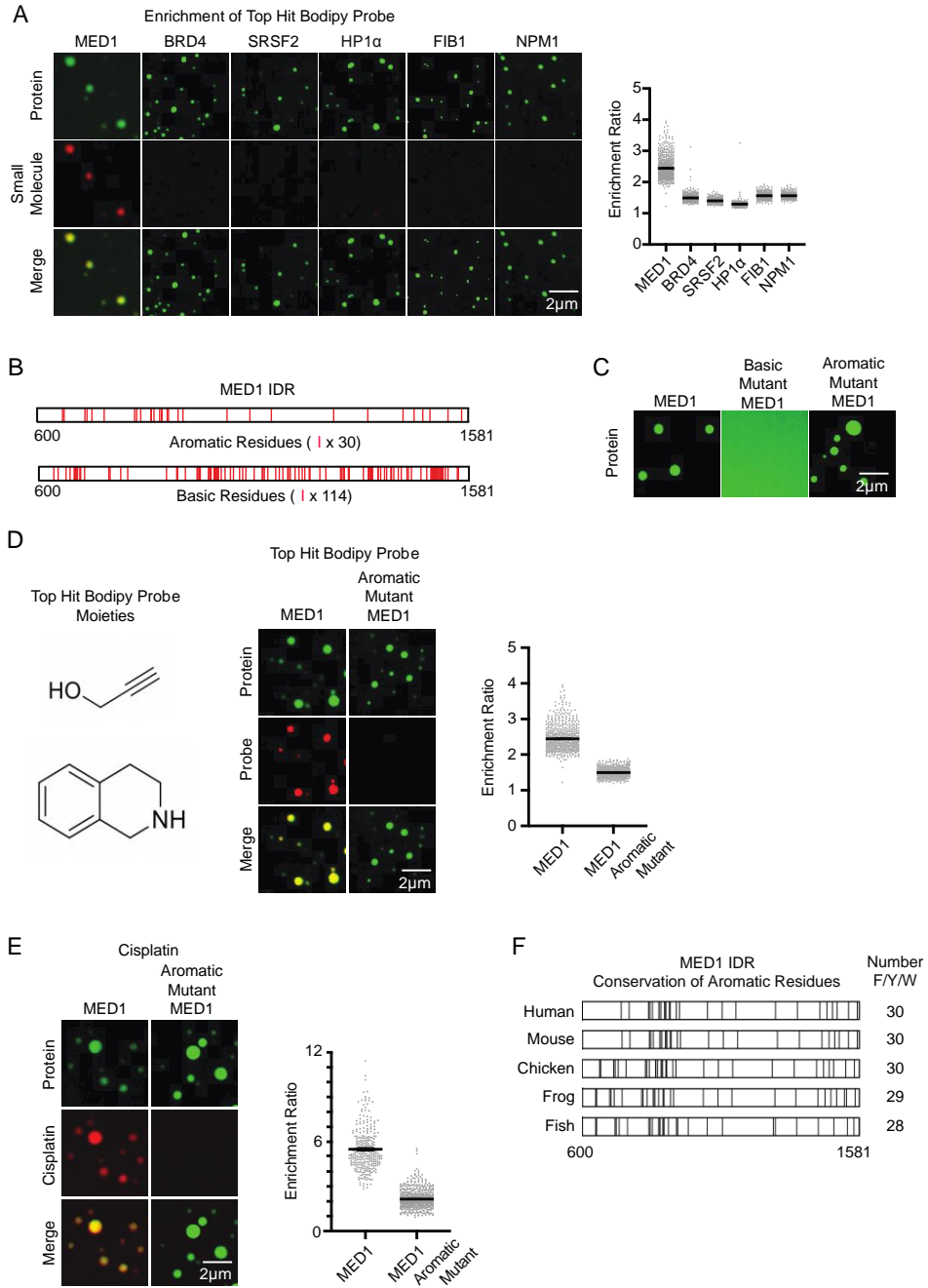


Figure S14. Aromatic residues of MED1 contribute to small molecule partitioning into MED1 condensates but are dispensable for condensate formation. (A) Confocal microscopy images of MED1, BRD4, SRSF2, HP1 $\alpha$ , FIB1, and NPM1 nuclear condensates formed in 125mM NaCl and 10% PEG together with 5 $\mu$ M of the small molecule probe that ranked the highest in fluorescent intensity within MED1 condensates. The probe was specifically concentrated into MED1 condensates, indicating that chemical features of the probe selectively interact with those of MED1 condensates. The top-ranking probes that concentrated in MED1 condensates showed a preference for BODIPY molecules that are modified with an aromatic ring. This suggests that the pi-system might be contributing to the interaction between small molecules and MED1. (B) Schematic of the MED1 IDR mutant proteins. The pi-system governs the interactions of supramolecular assemblies, where pi-pi or pi-cation interactions play prominent roles. To test if these interactions govern small molecule partitioning into MED1 condensates, and encouraged by the observation that the MED1 IDR is enriched for both aromatic and basic amino acids residues relative to other proteins studied here (Figure S3B), we generated an aromatic MED1 IDR mutant (all 30 aromatic residues changed to alanine) and a basic MED1 IDR mutant (all 114 basic residues changed to alanine). (C) We tested the ability of MED1 mutants to form droplets by confocal microscopy using MED1 wildtype, MED1 basic mutant (all basic amino acids replaced with alanine), and MED1 aromatic mutant (all aromatic amino acids replaced with alanine) in the presence of 125mM NaCl and 10% PEG. The MED1 basic mutant showed an impaired ability to form droplets in vitro, indicating that the basic residues of MED1 are required for the homotypic interactions that govern droplet formation. The MED1 aromatic mutant formed droplets similar to those of MED1 wildtype protein. (D) Role of MED1 aromatic residues in incorporation of aromatic small molecule probes. Confocal microscopy images and their quantification for the top hit BODIPY probe together with

MED1 or MED1 aromatic mutant, which show that the partitioning behavior of the aromatic probe into MED1 aromatic mutant droplets is substantially reduced. Experiments were performed in 10% PEG and 125mM NaCl with 10 $\mu$ M protein and 5 $\mu$ M small molecule. (E) Confocal microscopy images and their quantification for cisplatin together with MED1 or MED1 aromatic mutant, which show that the partitioning behavior of cisplatin into MED1 aromatic mutant droplets is substantially reduced. Experiments were performed in 10% PEG and 125mM NaCl with 10 $\mu$ M protein and 5 $\mu$ M cisplatin-TR. Taken together, these results suggest that the pi-system contributes to small molecule partitioning into MED1 condensates. (F) Conservation of aromatic amino acids in the MED1 IDR across species, with the total number of aromatic residues for each species. All error bars represent SEM.

**Fig. S15.**

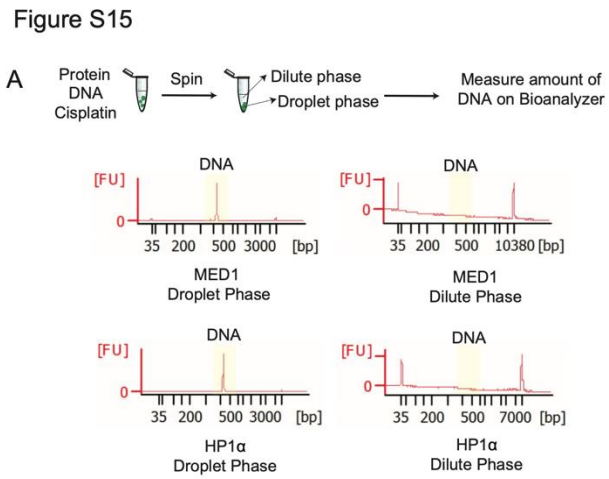


Figure S15. DNA can be compartmentalized and concentrated in nuclear condensates. (Top) Schematic of droplet assay showing protein, DNA, and cisplatin mixed in droplet forming conditions, then spun down to separate the droplet phase from the dilute phase. The amount of DNA in the two phases is subsequently measured using a Bioanalyzer. DNA is enriched in MED1 and HP1 $\alpha$  droplet phase (left) compared to MED1 and HP1 $\alpha$  dilute phase (right).

**Fig. S16.**

Figure S16

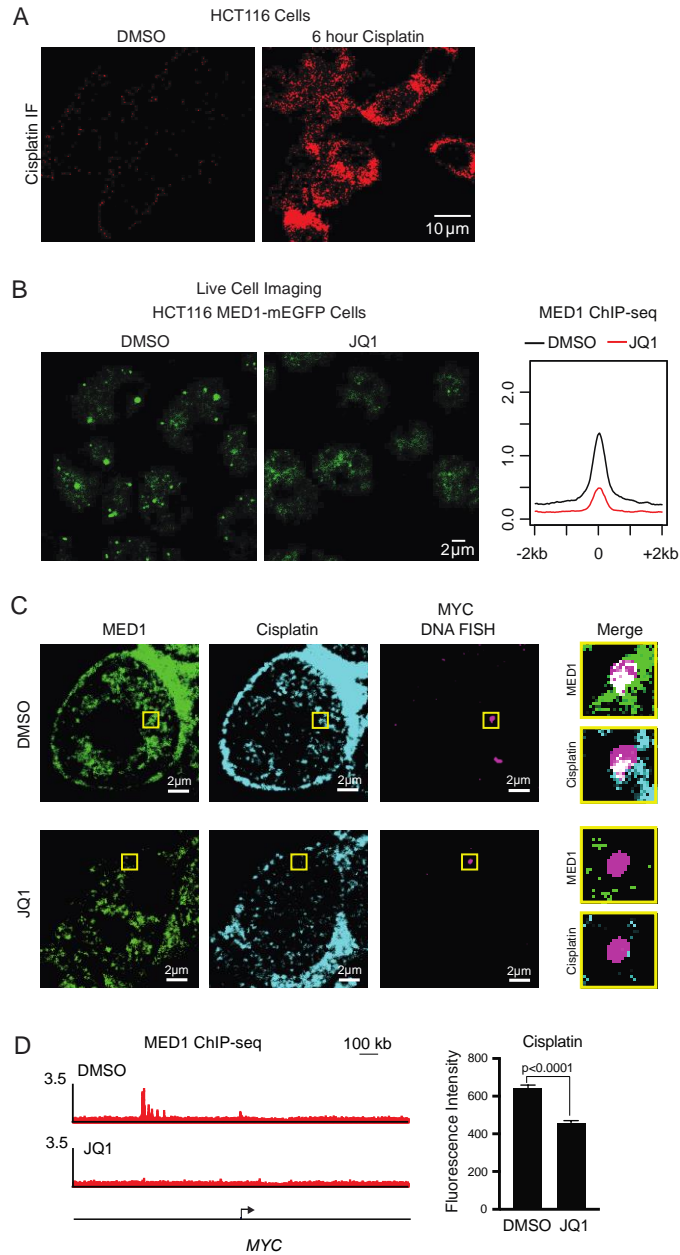


Figure S16. Concentration of small molecules in specific condensates can influence target engagement. (A) HCT116 cells were treated with DMSO or 50 $\mu$ M cisplatin for 6 hours followed by cisplatin immunofluorescence. The antibody only recognizes platinated DNA in cells treated

with cisplatin, supporting antibody specificity. (B) (Left) mEGFP-MED1 tagged HCT116 cells treated with JQ1 for 24 hours result in diminution of MED1 condensates. (Right) Metaplot of MED1 ChIP-Seq in DMSO vs JQ1 treated HCT116 cells. (C) Cells were treated with JQ1 and then cisplatin to determine whether diminution of MED1 condensates leads to reduced DNA platination at *MYC* locus. *MYC* DNA FISH and MED1 immunofluorescence showed a loss of signal for platinated DNA after JQ1 treatment, indicating that the presence of a MED1 condensate contributes to DNA platination at this locus. (D) (Left) MED1 ChIP-Seq track at *MYC* in DMSO or JQ1 treated HCT116 cell showing loss of MED1 loading after JQ1 treatment. (Right) Quantification of cisplatin IF signal at *MYC* DNA FISH foci in HCT116 cells with DMSO or JQ1 treatment, error bars represent SEM.

**Fig. S17.**

Figure S17

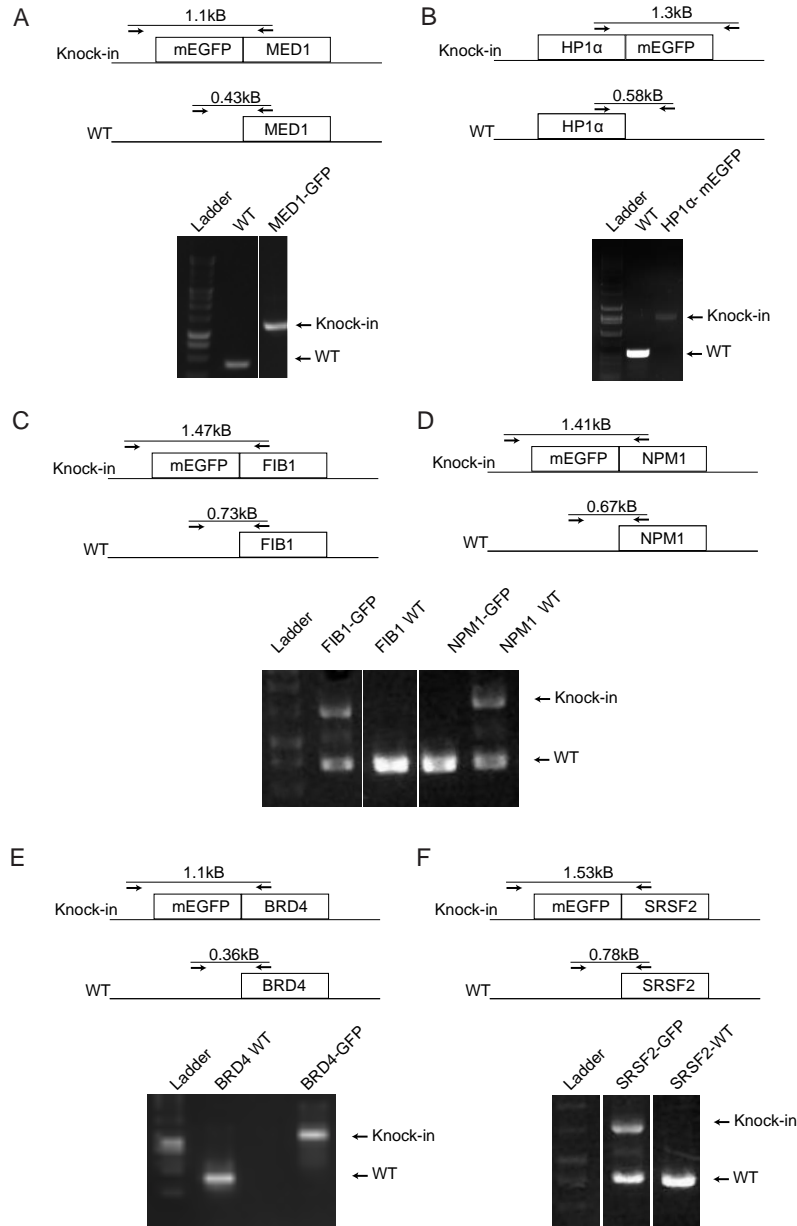


Figure S17. Genotyping of endogenously tagged cell lines. Schematic image and genotyping agarose gel showing mEGFP tagged (A) MED1, (B) HP1α, (C) FIB1 (D) NPM1, (E) BRD4, and (F) SRSF2 in HCT116 colon cancer cells.

**Fig. S18.**

Figure S18

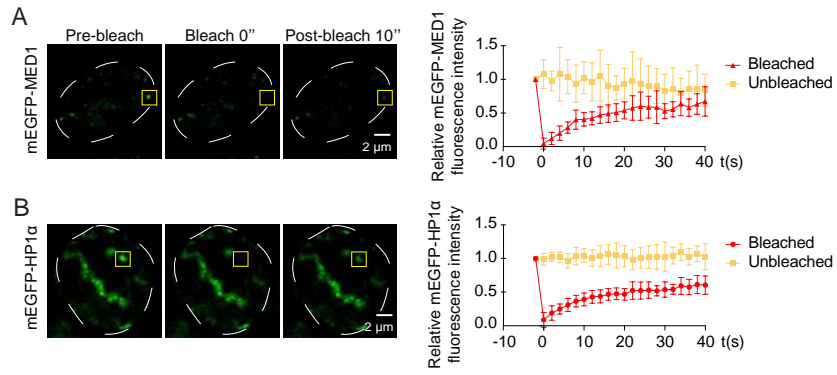


Figure S18. Nuclear condensates in cells are highly dynamic. FRAP of mEGFP-tagged (A) MED1 and (B) HP1 $\alpha$  in HCT116 cell lines (error bars represent SEM) (n=7).

**Fig. S19.**

Figure S19

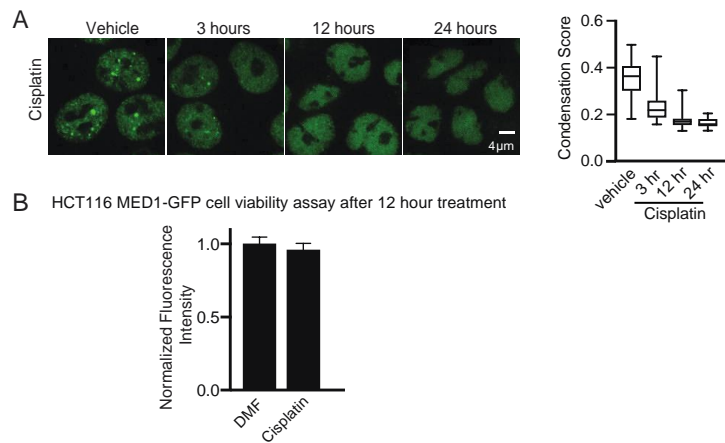


Figure S19. Dissolution of MED1 condensates in cells upon prolonged cisplatin treatment. (A) HCT116 cells endogenously GFP-tagged MED1 treated with DMF or 50μM cisplatin for 3, 6, or 12 hours. Quantification shown to the right, error bars are SD. (B) Cell viability assay of HCT116 cells expressing GFP-MED1 treated for 12 hours with DMF or 50μM Cisplatin.

**Fig. S20.**

Figure S20

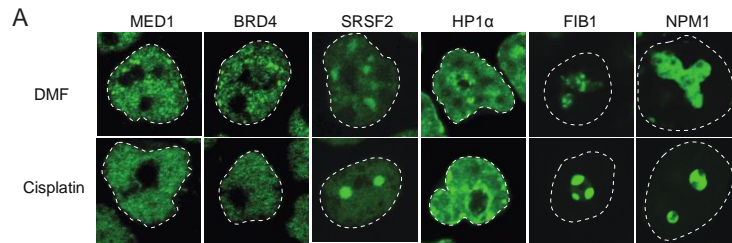


Figure S20. Effect of cisplatin on various nuclear condensates. (A) HCT116 cells bearing either endogenously GFP-tagged MED1, BRD4, HP1 $\alpha$ , FIB1, NPM1, or SRSF2 treated with 50 $\mu$ M cisplatin for 12 hours. Cisplatin specifically disrupts MED1 and BRD4 condensates, consistent with cisplatin and BRD4 being selectively concentrated in MED1 condensates.

**Fig. S21.**

Figure S21

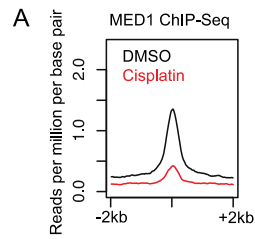


Figure S21. Decreased MED1 genomic occupancy upon cisplatin treatment. Graph shows MED1 ChIP-seq after 6 hours of DMSO or 50 $\mu$ M cisplatin treatment, MED1 genomic levels are reduced after cisplatin treatment.

**Fig. S22.**

**Figure S22**

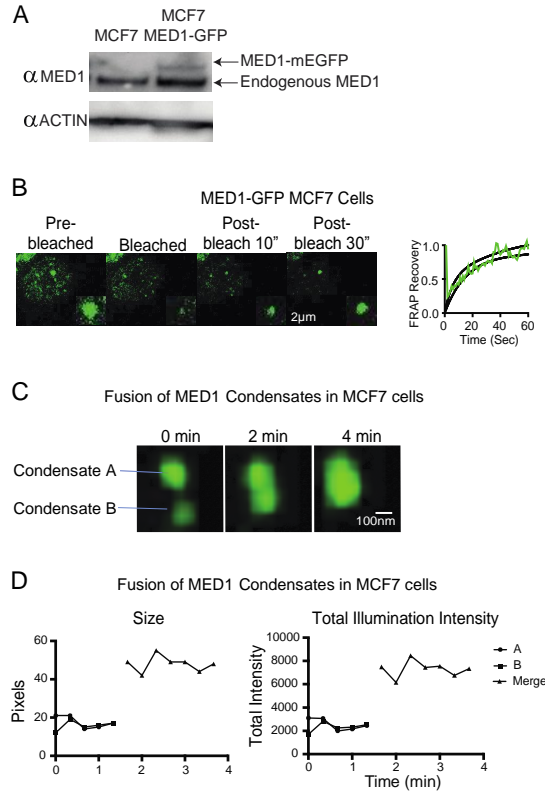


Figure S22. Characterization of MED1 condensates in MCF7 cells. (A) Western blot of MED1 in MCF7 cells and MCF cells infected with MED1-mEGFP lentiviral vector. (B) FRAP of MED1-mEGFP in MCF7 cells expressing this fusion protein by virtue of a lentiviral vector. Quantification shown to the right, black bars represent 95% confidence interval of the best fit line. (C) MCF7 cells expressing MED1-mEGFP were grown in estrogen-free conditions then stimulated with 100nM estrogen for 15 minutes and imaged for 4 minutes on a confocal fluorescent microscope. (D) Quantification of size and intensity of fusing MED1 condensates shown in (C).

Fig. S23.

Figure S23

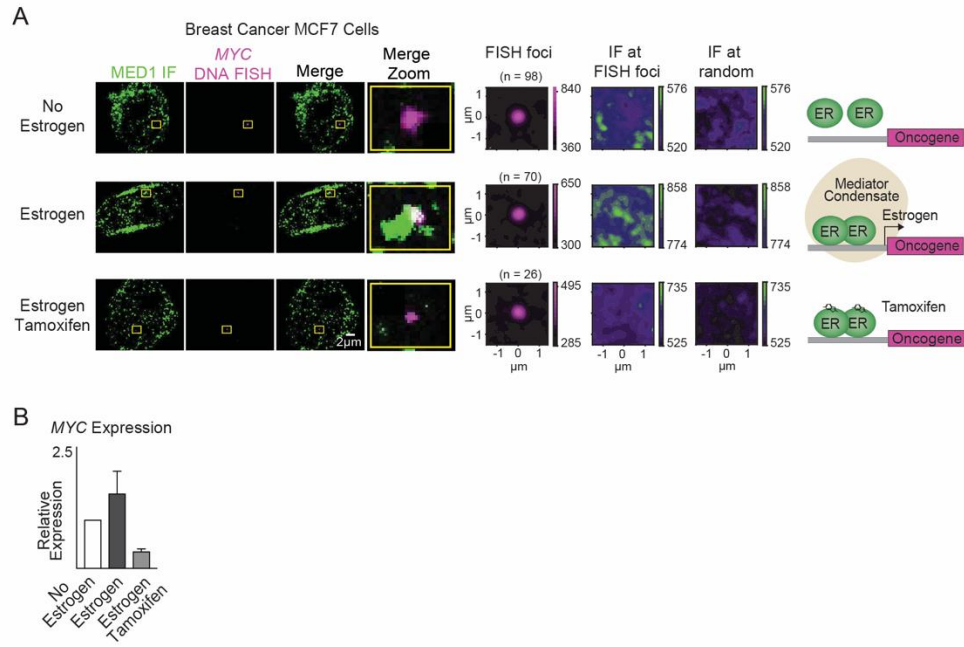


Figure S23. Estrogen and tamoxifen dependent MED1 condensate formation at the *MYC* oncogene. (A) DNA FISH and immunofluorescence in estrogen-starved MCF7 cells treated with 100nM estrogen or 100nM estrogen and 5 $\mu$ M tamoxifen for 24 hours. Average image analysis and random image analysis shown to the right. (B) RT-qPCR showing relative *MYC* RNA expression in estrogen-starved, estrogen stimulated, or estrogen and tamoxifen treated MCF7 cells, error bars represent SEM.

**Fig. S24.**

Figure S24

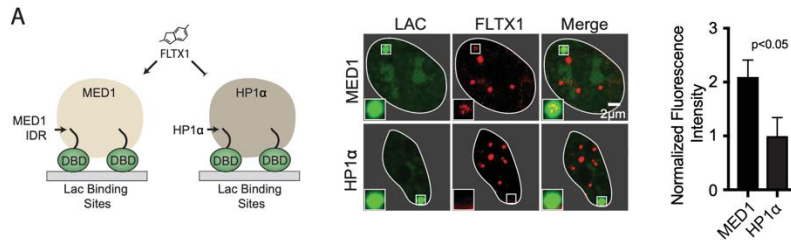


Figure S24. FLTX1 concentrates in MED1 condensates in cells. (Left) Schematic of MED1 or HP1 $\alpha$  tethered to the LAC array in U2OS cells generating a MED1 or HP1 $\alpha$  condensate. (Middle) Representative images of isolated U2OS cell nuclei with either MED1 or HP1 $\alpha$  tethered to the LAC array exposed to FLTX1. Zoomed image of the Lac array shown inset, merged images shown on the right. (Right) Quantification of FLTX1 enrichment at the LAC array with either MED1 or HP1 $\alpha$  tethered, error bars represent SEM. ESR1 is not expressed in this osteosarcoma cell line (67).

**Fig. S25.**

Figure S25

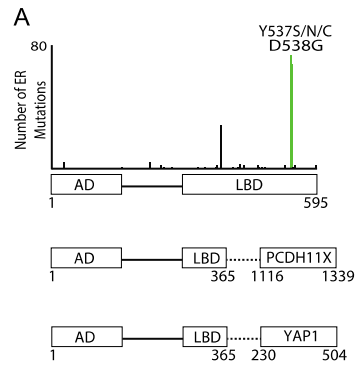


Figure S25. Patient derived hormonal therapy resistant mutations of ESR1. Plot of ER mutation frequency derived from a 220 patient set from the cBioPortal database showing locations of ER point mutations with hotspots at 537 and 538 (68).

**Fig. S26.**

Figure S26

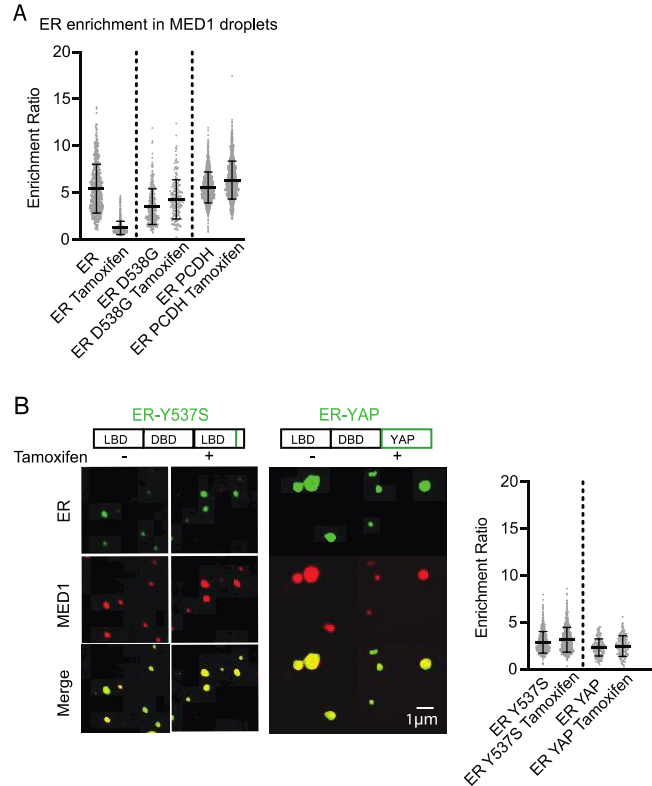


Figure S26. Enrichment ratios of ER and ER mutants in MED1 droplets. (A) Quantification of ER or ER mutant enrichment ratios in MED1 droplets in the presence of either estrogen or estrogen and tamoxifen. (B) (Left) Representative images of ER mutants partitioning in MED1 droplets, enrichment ratios shown to the right. Experiments for both (A) and (B) are performed in 125mM NaCl, 10% PEG, 10 $\mu$ M of each protein, 100 $\mu$ M estrogen with or without 100 $\mu$ M of the indicated ligand. All error bars represent SD.

**Fig. S27.**

Figure S27

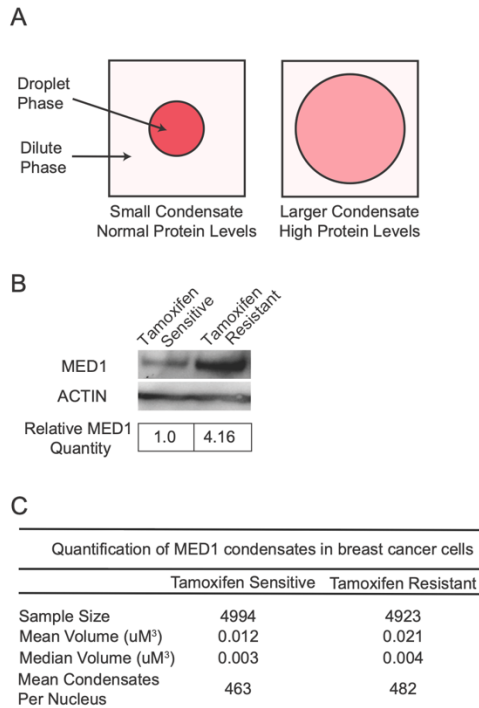


Figure S27. MED1 overexpression in tamoxifen resistant breast cancer cells. (A) Schematic demonstrating drug concentration in a condensate upon increase in condensate volume by scaffold protein overexpression. Assuming limited drug in a system (see Figure 4E), the concentration of drug in a MED1 droplet is expected to decrease upon condensate volume expansion (B) Western blot of MED1 and Actin in MCF7 cells (tamoxifen sensitive) and TAMR7 cells (tamoxifen resistant derivative of MCF7) showing that MED1 levels are higher TAMR7 cells. Quantification from the western blot is shown below, which is an average of 3 experiments. (C) Quantification of MED1 condensates in tamoxifen sensitive and resistant cell lines showing the volume of the MED1 condensates and the number of condensates per nucleus.

**Fig. S28.**

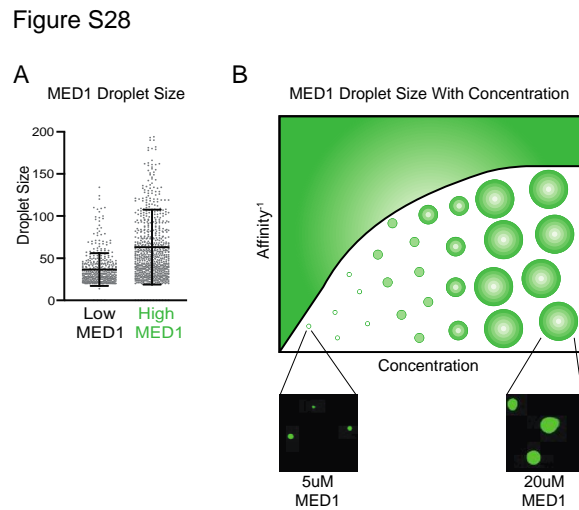


Figure S28. MED1 condensates increase in size with increasing MED1 concentration. (A) Droplet size in pixels from in vitro droplet assays performed with either 5 $\mu$ M (Low) or 20 $\mu$ M (High) MED1-GFP in 125mM NaCl and 10% PEG. Quantification shown to the right, error bars represent SD. (B) Schematic phase diagram of MED1, demonstrating that when the total concentration of MED1 increases, the size of droplet increases while maintaining the concentration of protein within the droplet phase.

**Fig. S29.**

Figure S29

A

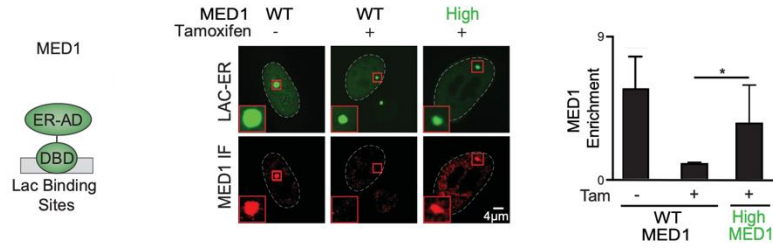


Figure S29. MED1 Condensation at the Lac Array. (A) (Left) Schematic of the Lac array assay. U2OS cells bearing 50,000 copies of the Lac binding site are transfected with a construct expressing the Lac DNA binding domain (DBD) to the estrogen receptor ligand binding domain (LBD). When the transcriptional apparatus is recruited to that site a mediator condensate is detectable by immunofluorescence (12) (Middle) U2OS-Lac cells were transfected with a construct expressing the Lac DBD fused to the ER LBD and GFP +/- a construct overexpressing MED1. Cells were grown in estrogen deprived media, and treated with 10nM estrogen +/- 10nM tamoxifen then fixed and subjected to MED1 IF. Top panel shows the location of ER-LBD at the Lac array, bottom panel shows MED1 IF. Inset image shows zoom. (Right) Quantification of MED1 enrichment relative at the Lac array, error bars represent SD.

**Fig. S30.**

Figure S30

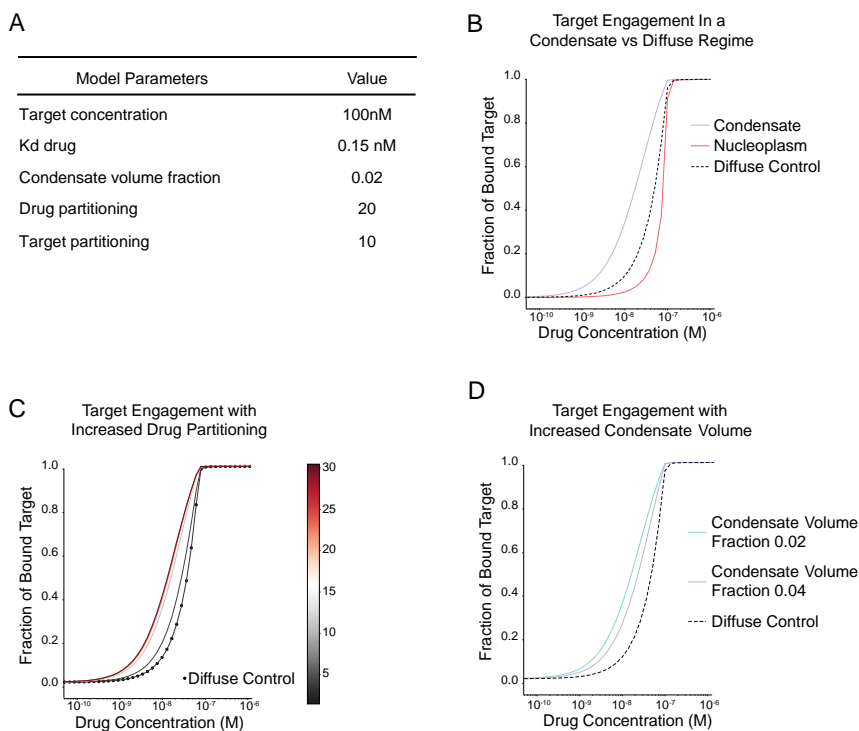


Figure S30. In silico model of small molecule partitioning in condensates. To demonstrate the behavior of a small molecule drug engaging a target contained within a condensate, we developed a simple model in which a drug and target are both contained within a condensate with percent target engagement as the readout. In this model, target partitioning is not affected by drug binding (A) Table of the values used to build a model of drug engagement within condensates, derived from known values of ER and tamoxifen. Condensate volume fraction value derived from analysis of MED1 IF on human ER+ breast carcinoma biopsies (Figure S1A). (B) Target binding as a function of drug concentration in simulations. The dashed line represents a system in which target and drug are freely diffusing through the cells. Red and blue lines represent a system in which target and drug are concentrated into a condensate. The blue line represents target engagement in

the condensate where the drug and target are concentrated, the red line represents target engagement in the dilute phase of the nucleoplasm. Overall, these data show that drug engages a higher percent of target molecules inside a condensate than outside, at a given concentration. (C) Fraction of bound target at a given concentration of drug at various partitioning coefficients of drug. Dotted line represents the target engagement in a diffuse regime. Overall, this simulation shows that as the partitioning coefficient of drug in a condensate increases the percent of target bound at a given concentration. (D) Target engagement by drug in the setting of larger condensates. Simulation of target binding as a function of drug concentration in the setting of normal condensate volume (2% of the volume of the nucleus) versus larger condensate volume (4% of the volume of the nucleus). Diffuse control shown by the dashed line. Overall, these data show that a drug may be less effective in binding its target in larger condensates.

## References and Notes

1. Y. Shin, C. P. Brangwynne, Liquid phase condensation in cell physiology and disease. *Science* **357**, eaaf4382 (2017). [doi:10.1126/science.aaf4382](https://doi.org/10.1126/science.aaf4382) [Medline](#)
2. S. F. Banani, H. O. Lee, A. A. Hyman, M. K. Rosen, Biomolecular condensates: Organizers of cellular biochemistry. *Nat. Rev. Mol. Cell Biol.* **18**, 285–298 (2017). [doi:10.1038/nrm.2017.7](https://doi.org/10.1038/nrm.2017.7) [Medline](#)
3. A. A. Hyman, C. A. Weber, F. Jülicher, Liquid-liquid phase separation in biology. *Annu. Rev. Cell Dev. Biol.* **30**, 39–58 (2014). [doi:10.1146/annurev-cellbio-100913-013325](https://doi.org/10.1146/annurev-cellbio-100913-013325) [Medline](#)
4. R. J. Ries, S. Zaccara, P. Klein, A. Olarerin-George, S. Namkoong, B. F. Pickering, D. P. Patil, H. Kwak, J. H. Lee, S. R. Jaffrey, m<sup>6</sup>A enhances the phase separation potential of mRNA. *Nature* **571**, 424–428 (2019). [doi:10.1038/s41586-019-1374-1](https://doi.org/10.1038/s41586-019-1374-1) [Medline](#)
5. E. M. Langdon, A. S. Gladfelter, A new lens for RNA localization: Liquid-liquid phase separation. *Annu. Rev. Microbiol.* **72**, 255–271 (2018). [doi:10.1146/annurev-micro-090817-062814](https://doi.org/10.1146/annurev-micro-090817-062814) [Medline](#)
6. E. M. Langdon, Y. Qiu, A. Ghanbari Niaki, G. A. McLaughlin, C. A. Weidmann, T. M. Gerbich, J. A. Smith, J. M. Crutchley, C. M. Termini, K. M. Weeks, S. Myong, A. S. Gladfelter, mRNA structure determines specificity of a polyQ-driven phase separation. *Science* **360**, 922–927 (2018). [doi:10.1126/science.aar7432](https://doi.org/10.1126/science.aar7432) [Medline](#)
7. M.-T. Wei, Y.-C. Chang, S. F. Shimobayashi, Y. Shin, C. P. Brangwynne, Nucleated transcriptional condensates amplify gene expression. bioRxiv 737387 [Preprint]. 21 August 2019; <https://doi.org/10.1101/737387>.
8. T. J. J. Nott, E. Petsalaki, P. Farber, D. Jarvis, E. Fussner, A. Plochowitz, T. D. Craggs, D. P. Bazett-Jones, T. Pawson, J. D. D. Forman-Kay, A. J. J. Baldwin, Phase transition of a disordered nuage protein generates environmentally responsive membraneless organelles. *Mol. Cell* **57**, 936–947 (2015). [doi:10.1016/j.molcel.2015.01.013](https://doi.org/10.1016/j.molcel.2015.01.013) [Medline](#)
9. T. J. Nott, T. D. Craggs, A. J. Baldwin, Membraneless organelles can melt nucleic acid duplexes and act as biomolecular filters. *Nat. Chem.* **8**, 569–575 (2016). [doi:10.1038/nchem.2519](https://doi.org/10.1038/nchem.2519) [Medline](#)
10. B. R. Sabari, A. Dall’Agnese, A. Boija, I. A. Klein, E. L. Coffey, K. Shrinivas, B. J. Abraham, N. M. Hannett, A. V. Zamudio, J. C. Manteiga, C. H. Li, Y. E. Guo, D. S. Day, J. Schuijers, E. Vasile, S. Malik, D. Hnisz, T. I. Lee, I. I. Cisse, R. G. Roeder, P. A. Sharp, A. K. Chakraborty, R. A. Young, Coactivator condensation at super-enhancers links phase separation and gene control. *Science* **361**, eaar3958 (2018). [doi:10.1126/science.aar3958](https://doi.org/10.1126/science.aar3958) [Medline](#)
11. Y. E. Guo, J. C. Manteiga, J. E. Henninger, B. R. Sabari, A. Dall’Agnese, N. M. Hannett, J.-H. Spille, L. K. Afeyan, A. V. Zamudio, K. Shrinivas, B. J. Abraham, A. Boija, T.-M. Decker, J. K. Rimel, C. B. Fant, T. I. Lee, I. I. Cisse, P. A. Sharp, D. J. Taatjes, R. A. Young, Pol II phosphorylation regulates a switch between transcriptional and splicing condensates. *Nature* **572**, 543–548 (2019). [doi:10.1038/s41586-019-1464-0](https://doi.org/10.1038/s41586-019-1464-0) [Medline](#)
12. A. Boija, I. A. Klein, B. R. Sabari, A. Dall’Agnese, E. L. Coffey, A. V. Zamudio, C. H. Li, K. Shrinivas, J. C. Manteiga, N. M. Hannett, B. J. Abraham, L. K. Afeyan, Y. E. Guo, J.

- K. Rimel, C. B. Fant, J. Schuijers, T. I. Lee, D. J. Taatjes, R. A. Young, Transcription factors activate genes through the phase-separation capacity of their activation domains. *Cell* **175**, 1842–1855.e16 (2018). [doi:10.1016/j.cell.2018.10.042](https://doi.org/10.1016/j.cell.2018.10.042) [Medline](#)
13. J. J. Bouchard, J. H. Otero, D. C. Scott, E. Szulc, E. W. Martin, N. Sabri, D. Granata, M. R. Marzahn, K. Lindorff-Larsen, X. Salvatella, B. A. Schulman, T. Mittag, Cancer mutations of the tumor suppressor SPOP disrupt the formation of active, phase-separated compartments. *Mol. Cell* **72**, 19–36.e8 (2018). [doi:10.1016/j.molcel.2018.08.027](https://doi.org/10.1016/j.molcel.2018.08.027) [Medline](#)
  14. K. Shrinivas, B. R. Sabari, E. L. Coffey, I. A. Klein, A. Boija, A. V. Zamudio, J. Schuijers, N. M. Hannett, P. A. Sharp, R. A. Young, A. K. Chakraborty, Enhancer features that drive formation of transcriptional condensates. *Mol. Cell* **75**, 549–561.e7 (2019). [doi:10.1016/j.molcel.2019.07.009](https://doi.org/10.1016/j.molcel.2019.07.009) [Medline](#)
  15. E. P. Bentley, B. B. Frey, A. A. Deniz, Physical chemistry of cellular liquid-phase separation. *Chemistry* **25**, 5600–5610 (2019). [doi:10.1002/chem.201805093](https://doi.org/10.1002/chem.201805093) [Medline](#)
  16. M. Boehning, C. Dugast-Darzacq, M. Rankovic, A. S. Hansen, T. Yu, H. Marie-Nelly, D. T. McSwiggen, G. Kokic, G. M. Dailey, P. Cramer, X. Darzacq, M. Zweckstetter, RNA polymerase II clustering through carboxy-terminal domain phase separation. *Nat. Struct. Mol. Biol.* **25**, 833–840 (2018). [doi:10.1038/s41594-018-0112-y](https://doi.org/10.1038/s41594-018-0112-y) [Medline](#)
  17. P. Cramer, Organization and regulation of gene transcription. *Nature* **573**, 45–54 (2019). [doi:10.1038/s41586-019-1517-4](https://doi.org/10.1038/s41586-019-1517-4) [Medline](#)
  18. S. Alberti, S. Saha, J. B. Woodruff, T. M. Franzmann, J. Wang, A. A. Hyman, A user's guide for phase separation assays with purified proteins. *J. Mol. Biol.* **430**, 4806–4820 (2018). [doi:10.1016/j.jmb.2018.06.038](https://doi.org/10.1016/j.jmb.2018.06.038) [Medline](#)
  19. D. Hnisz, K. Shrinivas, R. A. Young, A. K. Chakraborty, P. A. Sharp, A phase separation model for transcriptional control. *Cell* **169**, 13–23 (2017). [doi:10.1016/j.cell.2017.02.007](https://doi.org/10.1016/j.cell.2017.02.007) [Medline](#)
  20. Y. Chen, A. S. Belmont, Genome organization around nuclear speckles. *Curr. Opin. Genet. Dev.* **55**, 91–99 (2019). [doi:10.1016/j.gde.2019.06.008](https://doi.org/10.1016/j.gde.2019.06.008) [Medline](#)
  21. A. G. Larson, D. Elnatan, M. M. Keenen, M. J. Trnka, J. B. Johnston, A. L. Burlingame, D. A. Agard, S. Redding, G. J. Narlikar, Liquid droplet formation by HP1 $\alpha$  suggests a role for phase separation in heterochromatin. *Nature* **547**, 236–240 (2017). [doi:10.1038/nature22822](https://doi.org/10.1038/nature22822) [Medline](#)
  22. A. R. Strom, A. V. Emelyanov, M. Mir, D. V. Fyodorov, X. Darzacq, G. H. Karpen, Phase separation drives heterochromatin domain formation. *Nature* **547**, 241–245 (2017). [doi:10.1038/nature22989](https://doi.org/10.1038/nature22989) [Medline](#)
  23. M. Feric, N. Vaidya, T. S. Harmon, D. M. Mitrea, L. Zhu, T. M. Richardson, R. W. Kriwacki, R. V. Pappu, C. P. Brangwynne, Coexisting liquid phases underlie nucleolar subcompartments. *Cell* **165**, 1686–1697 (2016). [doi:10.1016/j.cell.2016.04.047](https://doi.org/10.1016/j.cell.2016.04.047) [Medline](#)
  24. D. M. Mitrea, J. A. Cika, C. S. Guy, D. Ban, P. R. Banerjee, C. B. Stanley, A. Nourse, A. A. Deniz, R. W. Kriwacki, Nucleophosmin integrates within the nucleolus via multi-modal interactions with proteins displaying R-rich linear motifs and rRNA. *eLife* **5**, e13571 (2016). [doi:10.7554/eLife.13571](https://doi.org/10.7554/eLife.13571) [Medline](#)

25. D. M. Mitrea, J. A. Cika, C. B. Stanley, A. Nourse, P. L. Onuchic, P. R. Banerjee, A. H. Phillips, C.-G. Park, A. A. Deniz, R. W. Kriwacki, Self-interaction of NPM1 modulates multiple mechanisms of liquid-liquid phase separation. *Nat. Commun.* **9**, 842 (2018). [doi:10.1038/s41467-018-03255-3](https://doi.org/10.1038/s41467-018-03255-3) [Medline](#)
26. S. F. Banani, A. M. Rice, W. B. Peeples, Y. Lin, S. Jain, R. Parker, M. K. Rosen, Compositional control of phase-separated cellular bodies. *Cell* **166**, 651–663 (2016). [doi:10.1016/j.cell.2016.06.010](https://doi.org/10.1016/j.cell.2016.06.010) [Medline](#)
27. A. Patel, H. O. O. Lee, L. Jawerth, S. Maharana, M. Jahnel, M. Y. Y. Hein, S. Stoyanov, J. Mahamid, S. Saha, T. M. M. Franzmann, A. Pozniakovski, I. Poser, N. Maghelli, L. A. A. Royer, M. Weigert, E. W. W. Myers, S. Grill, D. Drechsel, A. A. A. Hyman, S. Alberti, A liquid-to-solid phase transition of the ALS protein FUS accelerated by disease mutation. *Cell* **162**, 1066–1077 (2015). [doi:10.1016/j.cell.2015.07.047](https://doi.org/10.1016/j.cell.2015.07.047) [Medline](#)
28. S. Alberti, The wisdom of crowds: Regulating cell function through condensed states of living matter. *J. Cell Sci.* **130**, 2789–2796 (2017). [doi:10.1242/jcs.200295](https://doi.org/10.1242/jcs.200295) [Medline](#)
29. A. E. Posey, A. S. Holehouse, R. V. Pappu, “Chapter one - phase separation of intrinsically disordered proteins,” in *Methods in Enzymology* (Elsevier, 2018), vol. 611, pp. 1–30.
30. V. N. Uversky, Intrinsically disordered proteins in overcrowded milieu: Membrane-less organelles, phase separation, and intrinsic disorder. *Curr. Opin. Struct. Biol.* **44**, 18–30 (2017). [doi:10.1016/j.sbi.2016.10.015](https://doi.org/10.1016/j.sbi.2016.10.015) [Medline](#)
31. Y. S. Mao, B. Zhang, D. L. Spector, Biogenesis and function of nuclear bodies. *Trends Genet.* **27**, 295–306 (2011). [doi:10.1016/j.tig.2011.05.006](https://doi.org/10.1016/j.tig.2011.05.006) [Medline](#)
32. D. Hnisz, B. J. Abraham, T. I. Lee, A. Lau, V. Saint-André, A. A. Sigova, H. A. Hoke, R. A. Young, Super-enhancers in the control of cell identity and disease. *Cell* **155**, 934–947 (2013). [doi:10.1016/j.cell.2013.09.053](https://doi.org/10.1016/j.cell.2013.09.053) [Medline](#)
33. Y. H. Chu, M. Sibrian-Vazquez, J. O. Escobedo, A. R. Phillips, D. T. Dickey, Q. Wang, M. Ralle, P. S. Steyger, R. M. Strongin, Systemic delivery and biodistribution of cisplatin in vivo. *Mol. Pharm.* **13**, 2677–2682 (2016). [doi:10.1021/acs.molpharmaceut.6b00240](https://doi.org/10.1021/acs.molpharmaceut.6b00240) [Medline](#)
34. S. Vibet, K. Mahéo, J. Goré, P. Dubois, P. Bougnoux, I. Chourpa, Differential subcellular distribution of mitoxantrone in relation to chemosensitization in two human breast cancer cell lines. *Drug Metab. Dispos.* **35**, 822–828 (2007). [doi:10.1124/dmd.106.013474](https://doi.org/10.1124/dmd.106.013474) [Medline](#)
35. P. J. Smith, H. R. Sykes, M. E. Fox, I. J. Furlong, Subcellular distribution of the anticancer drug mitoxantrone in human and drug-resistant murine cells analyzed by flow cytometry and confocal microscopy and its relationship to the induction of DNA damage. *Cancer Res.* **52**, 4000–4008 (1992). [Medline](#)
36. N. Kwiatkowski, T. Zhang, P. B. Rahl, B. J. Abraham, J. Reddy, S. B. Ficarro, A. Dastur, A. Amzallag, S. Ramaswamy, B. Tesar, C. E. Jenkins, N. M. Hannett, D. McMillin, T. Sanda, T. Sim, N. D. Kim, T. Look, C. S. Mitsiades, A. P. Weng, J. R. Brown, C. H. Benes, J. A. Marto, R. A. Young, N. S. Gray, Targeting transcription regulation in cancer with a covalent CDK7 inhibitor. *Nature* **511**, 616–620 (2014). [doi:10.1038/nature13393](https://doi.org/10.1038/nature13393) [Medline](#)

37. J. Marrero-Alonso, A. Morales, B. García Marrero, A. Boto, R. Marín, D. Cury, T. Gómez, L. Fernández-Pérez, F. Lahoz, M. Díaz, Unique SERM-like properties of the novel fluorescent tamoxifen derivative FLTX1. *Eur. J. Pharm. Biopharm.* **85** (3 Pt B), 898–910 (2013). [doi:10.1016/j.ejpb.2013.04.024](https://doi.org/10.1016/j.ejpb.2013.04.024) [Medline](#)
38. W.-K. Cho, J.-H. Spille, M. Hecht, C. Lee, C. Li, V. Grube, I. I. Cisse, Mediator and RNA polymerase II clusters associate in transcription-dependent condensates. *Science* **361**, 412–415 (2018). [doi:10.1126/science.aar4199](https://doi.org/10.1126/science.aar4199) [Medline](#)
39. M. J. Tilby, C. Johnson, R. J. Knox, J. Cordell, J. J. Roberts, C. J. Dean, Sensitive detection of DNA modifications induced by cisplatin and carboplatin in vitro and in vivo using a monoclonal antibody. *Cancer Res.* **51**, 123–129 (1991). [Medline](#)
40. X. Shu, X. Xiong, J. Song, C. He, C. Yi, Base-resolution analysis of cisplatin-DNA adducts at the genome scale. *Angew. Chem. Int. Ed.* **55**, 14246–14249 (2016). [doi:10.1002/anie.201607380](https://doi.org/10.1002/anie.201607380) [Medline](#)
41. W. A. Whyte, D. A. Orlando, D. Hnisz, B. J. Abraham, C. Y. Lin, M. H. Kagey, P. B. Rahl, T. I. Lee, R. A. Young, Master transcription factors and mediator establish super-enhancers at key cell identity genes. *Cell* **153**, 307–319 (2013). [doi:10.1016/j.cell.2013.03.035](https://doi.org/10.1016/j.cell.2013.03.035) [Medline](#)
42. X. Rovira-Clave, S. Jiang, Y. Bai, G. L. Barlow, S. Bhate, A. Coskun, G. Han, B. Zhu, C.-M. Ho, C. Hitzman, S.-Y. Chen, F.-A. Bava, G. Nolan, Subcellular localization of drug distribution by super-resolution ion beam imaging. bioRxiv 557603 [Preprint]. 22 February 2019; <https://doi.org/10.1101/557603>.
43. Y. Wang, T. Zhang, N. Kwiatkowski, B. J. Abraham, T. I. Lee, S. Xie, H. Yuzugullu, T. Von, H. Li, Z. Lin, D. G. Stover, E. Lim, Z. C. Wang, J. D. Iglehart, R. A. Young, N. S. Gray, J. J. Zhao, CDK7-dependent transcriptional addiction in triple-negative breast cancer. *Cell* **163**, 174–186 (2015). [doi:10.1016/j.cell.2015.08.063](https://doi.org/10.1016/j.cell.2015.08.063) [Medline](#)
44. M. R. Mansour, J. M. Abraham, L. Anders, A. Berezovskaya, A. Gutierrez, A. D. Durbin, J. Etchin, L. Lawton, S. E. Sallan, L. B. Silverman, M. L. Loh, S. P. Hunger, T. Sanda, R. A. Young, A. T. Look, B. J. Abraham, L. Anders, A. Berezovskaya, A. Gutierrez, A. D. Durbin, J. Etchin, L. Lawton, S. E. Sallan, L. B. Silverman, M. L. Loh, S. P. Hunger, T. Sanda, R. A. Young, A. T. Look, An oncogenic super-enhancer formed through somatic mutation of a noncoding intergenic element. *Science* **346**, 1373–1377 (2014).
45. J. E. Bradner, D. Hnisz, R. A. Young, Transcriptional addiction in cancer. *Cell* **168**, 629–643 (2017). [doi:10.1016/j.cell.2016.12.013](https://doi.org/10.1016/j.cell.2016.12.013) [Medline](#)
46. J. Lovén, H. A. Hoke, C. Y. Lin, A. Lau, D. A. Orlando, C. R. Vakoc, J. E. Bradner, T. I. Lee, R. A. Young, Selective inhibition of tumor oncogenes by disruption of super-enhancers. *Cell* **153**, 320–334 (2013). [doi:10.1016/j.cell.2013.03.036](https://doi.org/10.1016/j.cell.2013.03.036) [Medline](#)
47. Z. Nie, G. Hu, G. Wei, K. Cui, A. Yamane, W. Resch, R. Wang, D. R. Green, L. Tessarollo, R. Casellas, K. Zhao, D. Levens, c-Myc is a universal amplifier of expressed genes in lymphocytes and embryonic stem cells. *Cell* **151**, 68–79 (2012). [doi:10.1016/j.cell.2012.08.033](https://doi.org/10.1016/j.cell.2012.08.033) [Medline](#)
48. S. Dasari, P. B. Tchounwou, Cisplatin in cancer therapy: Molecular mechanisms of action. *Eur. J. Pharmacol.* **740**, 364–378 (2014). [doi:10.1016/j.ejphar.2014.07.025](https://doi.org/10.1016/j.ejphar.2014.07.025) [Medline](#)

49. D. Dubik, T. C. Dembinski, R. P. C. Shiu, Stimulation of c-myc oncogene expression associated with estrogen-induced proliferation of human breast cancer cells. *Cancer Res.* **47**, 6517–6521 (1987). [Medline](#)
50. A. Nagalingam, M. Tighiouart, L. Ryden, L. Joseph, G. Landberg, N. K. Saxena, D. Sharma, Med1 plays a critical role in the development of tamoxifen resistance. *Carcinogenesis* **33**, 918–930 (2012). [doi:10.1093/carcin/bgs105](https://doi.org/10.1093/carcin/bgs105) [Medline](#)
51. S. W. Fanning, C. G. Mayne, V. Dharmarajan, K. E. Carlson, T. A. Martin, S. J. Novick, W. Toy, B. Green, S. Panchamukhi, B. S. Katzenellenbogen, E. Tajkhorshid, P. R. Griffin, Y. Shen, S. Chandralapaty, J. A. Katzenellenbogen, G. L. Greene, Estrogen receptor alpha somatic mutations Y537S and D538G confer breast cancer endocrine resistance by stabilizing the activating function-2 binding conformation. *eLife* **5**, e12792 (2016). [doi:10.7554/eLife.12792](https://doi.org/10.7554/eLife.12792) [Medline](#)
52. C. S. Ross-Innes, R. Stark, A. E. Teschendorff, K. A. Holmes, H. R. Ali, M. J. Dunning, G. D. Brown, O. Gojis, I. O. Ellis, A. R. Green, S. Ali, S. F. Chin, C. Palmieri, C. Caldas, J. S. Carroll, Differential oestrogen receptor binding is associated with clinical outcome in breast cancer. *Nature* **481**, 389–393 (2012). [doi:10.1038/nature10730](https://doi.org/10.1038/nature10730) [Medline](#)
53. M. Murtaza, S. J. Dawson, D. W. Y. Tsui, D. Gale, T. Forshew, A. M. Piskorz, C. Parkinson, S. F. Chin, Z. Kingsbury, A. S. C. Wong, F. Marass, S. Humphray, J. Hadfield, D. Bentley, T. M. Chin, J. D. Brenton, C. Caldas, N. Rosenfeld, Non-invasive analysis of acquired resistance to cancer therapy by sequencing of plasma DNA. *Nature* **497**, 108–112 (2013). [doi:10.1038/nature12065](https://doi.org/10.1038/nature12065) [Medline](#)
54. J. Cui, K. Germer, T. Wu, J. Wang, J. Luo, S. C. Wang, Q. Wang, X. Zhang, Cross-talk between HER2 and MED1 regulates tamoxifen resistance of human breast cancer cells. *Cancer Res.* **72**, 5625–5634 (2012). [doi:10.1158/0008-5472.CAN-12-1305](https://doi.org/10.1158/0008-5472.CAN-12-1305) [Medline](#)
55. S. Hole, A. M. Pedersen, S. K. Hansen, J. Lundqvist, C. W. Yde, A. E. Lykkesfeldt, New cell culture model for aromatase inhibitor-resistant breast cancer shows sensitivity to fulvestrant treatment and cross-resistance between letrozole and exemestane. *Int. J. Oncol.* **46**, 1481–1490 (2015). [doi:10.3892/ijo.2015.2850](https://doi.org/10.3892/ijo.2015.2850) [Medline](#)
56. L. Zhang, J. C. Er, H. Jiang, X. Li, Z. Luo, T. Ramezani, Y. Feng, M. K. Tang, Y. T. Chang, M. Vendrell, A highly selective fluorogenic probe for the detection and in vivo imaging of Cu/Zn superoxide dismutase. *Chem. Commun.* **52**, 9093–9096 (2016). [doi:10.1039/C6CC00095A](https://doi.org/10.1039/C6CC00095A) [Medline](#)
57. K. D. Meyer, A. J. Donner, M. T. Knuesel, A. G. York, J. M. Espinosa, D. J. Taatjes, Cooperative activity of cdk8 and GCN5L within Mediator directs tandem phosphoacetylation of histone H3. *EMBO J.* **27**, 1447–1457 (2008). [doi:10.1038/emboj.2008.78](https://doi.org/10.1038/emboj.2008.78) [Medline](#)
58. B. Langmead, S. L. Salzberg, Fast gapped-read alignment with Bowtie 2. *Nat. Methods* **9**, 357–359 (2012). [doi:10.1038/nmeth.1923](https://doi.org/10.1038/nmeth.1923) [Medline](#)
59. W. A. Whyte, S. Bilodeau, D. A. Orlando, H. A. Hoke, G. M. Frampton, C. T. Foster, S. M. Cowley, R. A. Young, Enhancer decommissioning by LSD1 during embryonic stem cell differentiation. *Nature* **482**, 221–225 (2012). [doi:10.1038/nature10805](https://doi.org/10.1038/nature10805) [Medline](#)
60. M. Rubinstein, R. H. Colby, *Polymer Physics* (Oxford Univ. Press, 2003).

61. M. Mittasch, P. Gross, M. Nestler, A. W. Fritsch, C. Iserman, M. Kar, M. Munder, A. Voigt, S. Alberti, S. W. Grill, M. Kreysing, Non-invasive perturbations of intracellular flow reveal physical principles of cell organization. *Nat. Cell Biol.* **20**, 344–351 (2018). [doi:10.1038/s41556-017-0032-9](https://doi.org/10.1038/s41556-017-0032-9) [Medline](#)
62. H. Zhao, P. H. Brown, P. Schuck, On the distribution of protein refractive index increments. *Biophys. J.* **100**, 2309–2317 (2011). [doi:10.1016/j.bpj.2011.03.004](https://doi.org/10.1016/j.bpj.2011.03.004) [Medline](#)
63. C. W. Pak, M. Kosno, A. S. Holehouse, S. B. Padrick, A. Mittal, R. Ali, A. A. Yunus, D. R. Liu, R. V. Pappu, M. K. Rosen, Sequence determinants of intracellular phase separation by complex coacervation of a disordered protein. *Mol. Cell* **63**, 72–85 (2016). [doi:10.1016/j.molcel.2016.05.042](https://doi.org/10.1016/j.molcel.2016.05.042) [Medline](#)
64. A. S. Holehouse, R. K. Das, J. N. Ahad, M. O. G. Richardson, R. V. Pappu, CIDER: Resources to analyze sequence-ensemble relationships of intrinsically disordered proteins. *Biophys. J.* **112**, 16–21 (2017). [doi:10.1016/j.bpj.2016.11.3200](https://doi.org/10.1016/j.bpj.2016.11.3200) [Medline](#)
65. M.-T. Wei, S. Elbaum-Garfinkle, A. S. Holehouse, C. C.-H. Chen, M. Feric, C. B. Arnold, R. D. Priestley, R. V. Pappu, C. P. Brangwynne, Phase behaviour of disordered proteins underlying low density and high permeability of liquid organelles. *Nat. Chem.* **9**, 1118–1125 (2017). [doi:10.1038/nchem.2803](https://doi.org/10.1038/nchem.2803) [Medline](#)
66. R. Delage-Mourroux, P. G. V. Martini, I. Choi, D. M. Kraichely, J. Hoeksema, B. S. Katzenellenbogen, Analysis of estrogen receptor interaction with a repressor of estrogen receptor activity (REA) and the regulation of estrogen receptor transcriptional activity by REA. *J. Biol. Chem.* **275**, 35848–35856 (2000). [doi:10.1074/jbc.M001327200](https://doi.org/10.1074/jbc.M001327200) [Medline](#)
67. Broad Institute, Cancer Cell Line Encyclopedia (CCLE); <https://portals.broadinstitute.org/ccle>.
68. cBioPortal for Cancer Genomics; <https://www.cbioportal.org/>.